Bioorganic Chemistry 140 (2023) 106794

Contents lists available at ScienceDirect

Bioorganic Chemistry

journal homepage: www.elsevier.com/locate/bioorg

Discovery of first novel sigma/HDACi dual-ligands with a potent *in vitro* antiproliferative activity

Carla Barbaraci [a,1], Viviana di Giacomo [b], Annalisa Maruca [c], Vincenzo Patamia [a], Roberta Rocca [c], Maria Dichiara [a], Annalisa Di Rienzo [b], Ivana Cacciatore [b], Amelia Cataldi [b], Marwa Balaha [b,d], Monica Rapino [e], Chiara Zagni [a], Daniele Zampieri [f], Lorella Pasquinucci [a], Carmela Parenti [a], Emanuele Amata [a], Antonio Rescifina [a], Stefano Alcaro [c,g,*], Agostino Marrazzo [a,*]

[a] Department of Drug and Health Sciences, Medicinal Chemistry Section, University of Catania, Viale Andrea Doria 6, 95125 Catania, Italy
[b] Department of Pharmacy, University "G. d'Annunzio", Chieti-Pescara, Via dei Vestini 31, 66100 Chieti, Italy
[c] Net4science academic spinoff srl, Università degli Studi "Magna Græcia" di Catanzaro, Campus "Salvatore Venuta", Viale Europa, 88100, Catanzaro, Italy
[d] Department of Pharmaceutical Chemistry, Faculty of Pharmacy, Kafrelsheikh University, Kafr El Sheikh 33516, Egypt
[e] Genetic Molecular Institute of CNR, Unit of Chieti, "G. d' Annunzio" University, Via dei Vestini 31, 66100 Chieti-Pescara, Italy
[f] Department of Chemical and Pharmaceutical Sciences, University of Trieste, Via Giorgieri 1, 34127 Trieste, Italy
[g] Dipartimento di Scienze della Salute, Università degli Studi "Magna Græcia" di Catanzaro, Campus "Salvatore Venuta", Viale Europa, 88100, Catanzaro, Italy

ARTICLE INFO

Keywords:
σ_1 Receptor
HDAC enzyme
Dual-Ligands
Multifactorial diseases
Cancer

ABSTRACT

Designing and discovering compounds for dual-target inhibitors is challenging to synthesize new, safer, and more efficient drugs than single-target drugs, especially to treat multifactorial diseases such as cancer. The simultaneous regulation of multiple targets might represent an alternative synthetic approach to optimize patient compliance and tolerance, minimizing the risk of target-based drug resistance due to the modulation of a few targets. To this end, we conceived for the first time the design and synthesis of dual-ligands σR/HDACi to evaluate possible employment as innovative candidates to address this complex disease. Among all synthesized compounds screened for several tumoral cell lines, compound **6** ($K_i\sigma_1R = 38 \pm 3.7$; $K_i\sigma_2R = 2917 \pm 769$ and HDACs $IC_{50} = 0.59$ μM) is the most promising candidate as an antiproliferative agent with an IC_{50} of 0.9 μM on the HCT116 cell line and no significant toxicity to normal cells. Studies of molecular docking, which confirmed the affinity over σ_1R and a pan-HDACs inhibitory behavior, support a possible balanced affinity and activity between both targets.

1. Introduction

Complex pathogenic mechanisms involving several targets and biochemical pathways regulate cancer and neurological disease. To treat these multifactorial pathologies, drugs addressing a single target could be inadequate compared to multi-targeting drug ligands (MTDLs) with more than one pharmacological activity [1,2]. In the last years, polypharmacology has emerged as a new paradigm in developing new synthetic compounds to treat multifactorial diseases and attain the desired physiological responses on specific targets [3].

Many traditional cytotoxic drugs interact specifically with their molecular targets, even though they are brutally labeled as "slash and burn" agents. Indeed, target-specific monotherapy leads to a single genetic alteration conferring target resistance to an individual tumor cell

Abbreviations: ER, endoplasmic reticulum; HDAC, histone deacetylases enzyme; HP, haloperidol; Hsp90, heat shock protein 90; MTDLs, multi-targeting drug ligands; NPC1, Niemann−Pick disease protein; σR, sigma receptors; SIRT, Sirtuin; TMEM97, the endoplasmic reticulum-resident transmembrane protein; VPA, valproic acid; ZBG, zinc binding group.

* Corresponding authors at: Net4science academic spinoff srl, Università degli Studi "Magna Græcia" di Catanzaro, Campus "Salvatore Venuta", Viale Europa, 88100, Catanzaro, Italy (Stefano Alcaro).

E-mail addresses: alcaro@unicz.it (S. Alcaro), marrazzo@unict.it (A. Marrazzo).

[1] C.B.- Laboratory of Medicinal Chemistry (CSIC, Associated Unit), Faculty of Pharmacy and Food Sciences and Institute of Biomedicine (IBUB), University of Barcelona, Av. Joan XXIII, 27-31, 08028 Barcelona, Spain.

https://doi.org/10.1016/j.bioorg.2023.106794
Received 19 April 2023; Received in revised form 9 August 2023; Accepted 15 August 2023
Available online 23 August 2023

and may eventually cause a relapse [4]. On the other hand, multi-targeted drugs, agents capable of modulating multiple targets simultaneously, pursue to maximize the chance for clinical antitumoral activity [5]. In particular, the clinical development of multi-ligand drugs presents the advantage of reducing drug resistance due to single-target mutations or expression changes, drug-drug interactions, therapeutic doses, and side effects, simplifying the pharmacokinetic profiles and improving therapeutic efficacy [6].

Sigma receptors (σRs) embody an enigmatic and unique class of chaperone proteins implicated in many pharmacological events, making them an attractive target proposed as a promising therapeutic treatment in various multifactorial diseases, including cancer therapy [7–9]. Identified as two subtypes, Sigma 1 (σ_1R) and Sigma 2 (σ_2R) receptors are distinguished by molecular weight, tissue distribution, ligand binding profile, pharmacology, and activation mechanisms. Widely distributed in the central nervous system, σ receptors were overexpressed in several human and rodent tumor cell lines, including breast, lung, prostate, colon, melanoma, neuroblastoma, and glioma[10]. Both receptors involve different biological functions, including cell proliferation and survival. The σ_1R has been purified, cloned, and crystallized [11] and well-characterized as a chaperone protein at the endoplasmic reticulum (ER)-mitochondria interface, where it regulates Ca^{2+} signaling and cell survival [12,13]. While the σ_1R agonists have shown neuroprotective, antiamnestic, and antidepressant effects [14,15], the σ_1R antagonists possess modulatory effects on opioid analgesia [16], analgesic, as well as antiproliferative and antiangiogenic activities [17–19]. The σ_2R, also identified as the endoplasmic reticulum-resident transmembrane protein TMEM97, regulates the sterol transporter Niemann–Pick disease protein (NPC1) [20], and has been recently crystallized [21]. Concerning the higher density than σ_1R in tumor cells [22], σ_2R has also been proposed as a possible biomarker for developing fluorescent and radiolabelled σR ligands in cancer diagnosis and therapy [23]. The σ ligands induce significant cell death and apoptosis only in tumor tissue and hardly in proliferating normal cells such as stem cells. Therefore, σ ligands may be used to selectively eradicate tumors as single agents or adjuvants in chemotherapy [24].

The inhibition of histone deacetylase enzymes (HDACs) was targeted for specific epigenetic changes associated with cancer and other diseases [25,26]. In nucleosome histone tail regions, HDACs catalyze the deacetylation of lysine residues, resulting in a more compacted chromatin structure that prevents transcription factors and RNA polymerase from accessing gene promoter regions, hence regulating gene expression [27]. HDACs also determine deacetylation in other proteins: tubulin, heat shock protein 90 (Hsp90), transcription factors, and DNA repair proteins [28]. HDACs can be distinguished respectively in two families and four classes. The zinc-dependent family is the most evaluated HDACs family, including 11 isoforms and divided into three classes: class-I (HDACs 1, 2, 3, and 8), class-II (further subdivided into IIa: HDACs 4, 5, 7, and 9, and IIb: HDACs 6 and 10), and class-IV (HDAC11). The second family depends on cofactor NAD^+ for its activity and includes only one class, sirtuins (SIRT1-7). Until now, more than twenty HDAC inhibitors (HDACis) have entered clinical studies (e.g., Entinostat) [29], and several of them (e.g., vorinostat, Panobinostat, romidepsin) [30–32] have been approved for the treatment of cutaneous *T*-cell lymphoma.

The growing interest in σ ligands as potential chemotherapeutic agents, followed by the encouraging results of HDACis in cancer therapy, headed to the development of ligands targeting σR and HDAC employing a prodrug approach to improve their anticancer capabilities [18,19,33]. Moreover, the recent employ of the modern approach based on polypharmacology or molecular hybridization in developing σR multiple-ligands [34] and multitarget HDACsi [35] for cancer, respectively, suggested the possibility of designing new dual-target compounds involving σR and HDAC enzyme simultaneously. Considering that a drug that "hits" multiple targets offers the potential for higher efficacy and lower off-target effects, we aimed to synthesize several compounds as "dual-ligands σR/HDAC" provide for a single chemical entity responsible for regulating both targets all at once. A preliminary screening on several tumoral cells permitted us to select the promising compounds for further pharmacological and computational studies, suggesting compounds **6** as the best candidate for a possible antitumoral treatment.

2. Results and discussion

2.1. Rational design

The new molecules designed as "dual-ligands" should be able to interact as such on the molecular targets considered, antagonizing the σ_1 receptor and inhibiting the HDAC enzyme. This means an appropriate, balanced affinity and activity between the two targets. A versatile approach to obtaining the desired dual-target candidate provides the combination of the appropriate pharmacophoric group common to both targets [36], leading to a single pharmacophore able to ensure optimal binding interaction either with the σ receptor or with the HDAC enzyme (Fig. 1).

The σR pharmacophore provides for the presence of certain essential functional groups: one nitrogen atom and two hydrophobic regions placed at an appropriate distance from the nitrogen atom [37,38]. However, the pharmacophore common to HDACis consists of a hydrophobic region that blocks access to the enzyme active site (capping group or CAP), a linker, and a functional group chelating the metal zinc (Zn^{2+}) at the bottom of the catalytic pocket (zinc binding group or ZBG), responsible for the enzyme's inhibition [39,40]. Hydroxamic acid and benzamide, recognized as ZBG functional groups in the structure of the well-know HDACi Panobinostat and Entinostat, were maintained in the structure of the designed compounds. In addition, a linker of a short methylene chain, including benzene as possible hydrophobic region II, was employed between the ZBG functional groups and the different amino moieties of well-known σ ligands representing the basic core essential for σR binding. These amino moieties are often connected with benzene, also substituted, which behaves in the hydrophobic region I common to both targets (Fig. 2A).

To explore multiple structural modifications, we wanted to simplify the structure of the new compounds with the design and synthesis of dual-ligands in which the amino moiety 4-(4-chlorophenyl)-4-hydroxypiperidine, nucleus of the well-known σ_1R antagonist Haloperidol (HP), and the benzamide group of Entinostat were separated each other just by a saturated hydrocarbon chain (Fig. 2B). The idea was to consider whether the benzamide group could act simultaneously as ZBG for HDAC inhibition and hydrophobic region II for improving the σR affinity, instead of the benzyl and/or saturated bound included in the others dual-ligands compounds. All the new dual-ligand compounds described above have been evaluated as possible candidates for anticancer therapy.

2.2. Synthesis

Compounds including the hydroxamic acid of Panobinostat or the benzamide group of Entinostat were synthesized, providing for esterification of *trans*-4-formilcinnamic acid with methyl iodide in *N*,*N*-dimethylformamide (DMF) to obtain the compound (*E*)-3-(4-formilphenyl)methyl acrylate. The latter was subjected to a reductive amination reaction with 4-benzylpiperazine in THF in the presence of $NaBH(OAc)_3$ and acetic acid to give the intermediate **3**. The hydrolysis of compound **3** and the subsequent reaction with *o*-phenylenediamine, in the presence of *N*-hydroxybenzotriazole (HOBt) and 1-ethyl-3-(3-dimethylaminopropyl)carbodiimide (EDC) supplied the final compound **4**. Instead, the hydrolysis of the **3** ester group in methanol and LiOH 1 M, followed by activation of the carboxylic acid with ethyl chloroformate and triethylamine (TEA) and nucleophilic reaction with

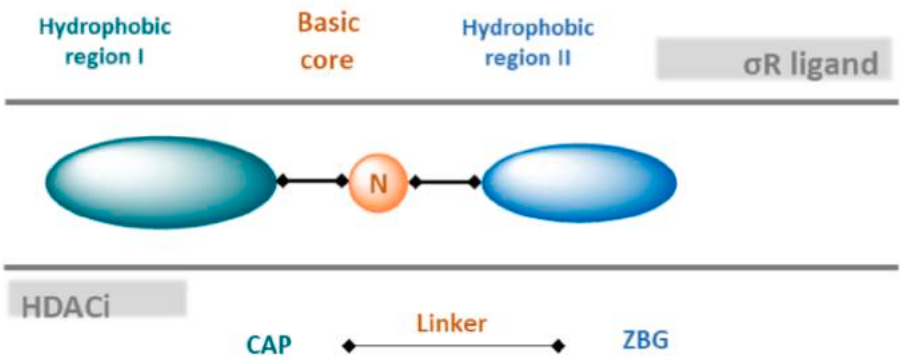

Fig. 1. Overlapping of the pharmacophoric models of σR and HDACi into a single one.

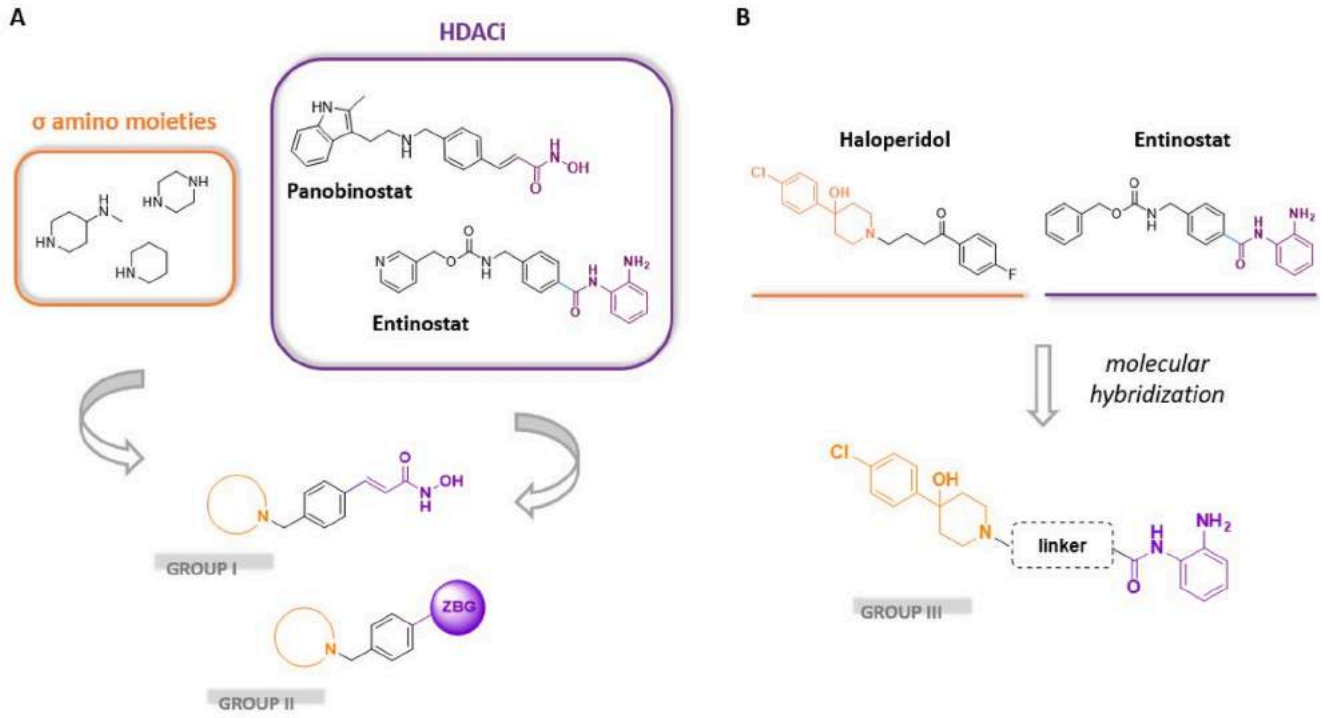

Fig. 2. Rational design of the sigma-HDACi dual-ligands.

O-(tetrahydro-2*H*-piran-2-yl)-hydroxylamine (NH_2OTHP) give the intermediate **5**. Finally, deprotection of the hydroxyl aminic group by hydrolysis with a solution of HCl 1.25 M in EtOH, provided the final product **6** (Scheme 1A). The second group of compounds was synthesized, providing a nucleophilic substitution of methyl-4-(bromomethyl)-benzoate with 4-benzylpiperazine or 1-benzyl-4-(methylamino)piperidine in EtOH to give the intermediates **8a**,**b**. The synthetic route to obtain the final products **9a**,**b**, and **11a**,**b** proceeds as previously described (Scheme 1B).

The general synthetic scheme of the third group of simplified benzamide derivatives, including HP and Entinostat cores previously described, involved the reaction between *o*-phenylenediamine and its appropriate acylic chloride in methylene chloride and the presence of TEA. Intermediate products **12a–c** were subjected to a nucleophilic substitution reaction with 4-(4-chlorophenyl)-4-hydroxypiperidine in DMF and K_2CO_3 to obtain the final compounds **13a–c** (Scheme 2).

2.3. Structure-affinity relationship studies

The synthesized compounds were evaluated for affinity at both σ_1R and σ_2R through a radioligand binding assay (Table 1). The lack of the benzamide-cinnamic group or hydroxyamino-cinnamic group's double bond in **9a** and **11a** leads to a loss of affinity for the σ_1R and improved selectivity over σ_2R. Moreover, a worsening of the affinity for σ_1R was observed for compounds including *o*-phenylenediamine **4** and **9a** ($K_i\sigma_1R$ = 1330 ± 239 and 3758 ± 929 nM, respectively) with respect to the corresponding compound with hydroxamic acid as ZBG **6** and **11a** ($K_i\sigma_1R$ = 38 ± 3.7 and 93 ± 10.9 nM, respectively). On the other hand, compounds **9b** ($K_i\sigma_1R$ = 52 ± 3.9 nM) showed just a decrease in affinity for σ_1R compared to **11b** ($K_i\sigma_1R$ = 41 ± 6.5 nM). All the compounds of these series showed a poor affinity for σ_2R, while **9a** and **11a**, including 4-benzylpiperazine moiety and without the double bound as mentioned above, completely lost the capacity to bind σ_2R ($K_i\sigma_2R$ > 10000 nM).

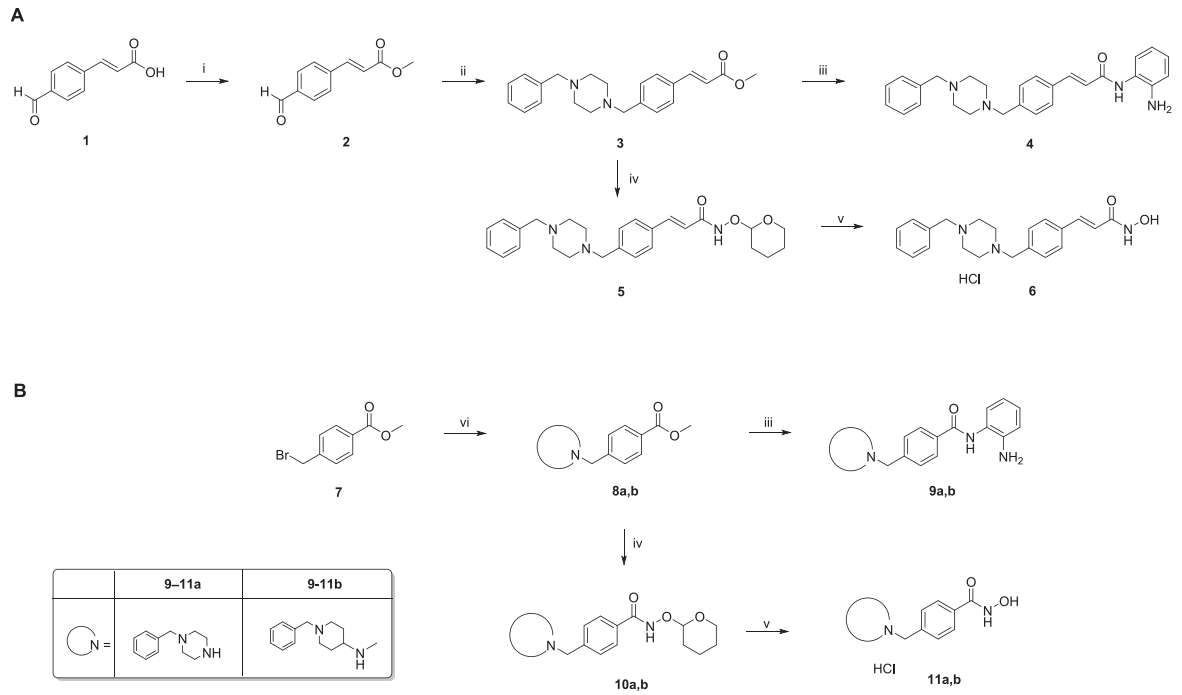

Scheme 1. Synthesis of compounds **4**, **6**, **9a**,**b** and **11a**,**b**. Reagents and conditions: (i) MeI, DMF, rt; (ii) 4-benzylpiperazine, AcOH, $NaBH(OAc)_3$, THF, rt; (iii) 1. LiOH 1 M, MeOH, rt; 2. *o*-phenylendiamine, HOBt, EDC, DMF; (iv) 1. LiOH 1 M, MeOH, rt; 2. $ClCO_2Et$, TEA, THF, rt; 3. NH_2OTHP, THF, rt; (v) HCl 1.25 M; (vi) 4-benzylpiperazine or 1-benzyl-4-(methylamino)piperidine, EtOH, $NaHCO_3$, 70 °C.

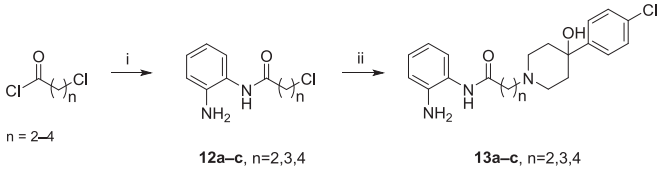

Scheme 2. Synthesis of compounds **13a**—**c**. Reagent and conditions: (i) *o*-phenylendiamine, TEA, CH_2Cl_2, rt; (ii) 4-(4-chlorophenyl)-4-hydroxypiperidine, K_2CO_3, DMF, 80 °C.

Despite a lower affinity over both σ receptors for all compounds, including *o*-phenylenediamine in the previous groups, the third series of dual-ligands restored the affinity towards σ_1R; in particular, increasing the chain length, the affinity toward σ_2R decreased, and the selectivity improves. Indeed, compound **13a** had a $K_i\sigma_1$R of 47 *vs*. $K_i\sigma_2$R of 738 nM, compound **13b** 55 nM for $K_i\sigma_1$R *vs*. 2799 nM for $K_i\sigma_2$R, while compound **13c** helds $K_i\sigma_1$R 107 nM and completely lost affinity for σ_2R with $K_i\sigma_2$R > 10000.

Table 1
The results of σ_1R and σ_2R binding assays for the sigma-HDACi dual-ligands.

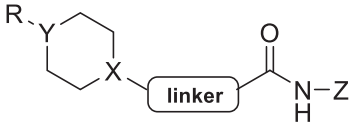

						K_i (nM) ± SD[a]	
Compd	R	Y	X	linker	Z	σ_1R	σ_2R
4	Bn	N	N	$CH_2PhCH=CH$	*o*-$NH_2C_6H_4$	1330 ± 239	2691 ± 1254
6	Bn	N	N	$CH_2PhCH=CH$	OH	38 ± 3.7	2917 ± 769
9a	Bn	N	N	$CH_2C_6H_4$	*o*-$NH_2C_6H_4$	3758 ± 929	>10000
9b	Bn	N	C	$N(CH_3)CH_2C_6H_4$	*o*-$NH_2C_6H_4$	52 ± 3.9	1588 ± 233
11a	Bn	N	N	$CH_2C_6H_4$	OH	93 ± 10.9	>10000
11b	Bn	N	C	$N(CH_3)CH_2C_6H_4$	OH	41 ± 6.5	166 ± 14.8
13a	*p*-ClC_6H_4	C-OH	N	$(CH_2)_2$	*o*-$NH_2C_6H_4$	47 ± 4.6	738 ± 117
13b	*p*-ClC_6H_4	C-OH	N	$(CH_2)_3$	*o*-$NH_2C_6H_4$	55 ± 3.2	2799 ± 609
13c	*p*-ClC_6H_4	C-OH	N	$(CH_2)_4$	*o*-$NH_2C_6H_4$	107 ± 17	>10000
HP						2.6 ± 0.4	77 ± 18
(+)-PTZ[b]						4.3 ± 0.5	1465 ± 224
DTG[b]						124 ± 19	18 ± 1
BD-1063[b]						14 ± 2.7	204 ± 31

[a] Each value is the mean ± SD of at least two experiments performed in duplicate. [b]PTZ = pentazocine, DTG = 1,3-di-*o*-tolylguanidine, BD1063 = 1-[2-(3,4-Dichlorophenyl)ethyl]-4-methylpiperazine dihydrochloride.

2.4. Effects of compounds on tumoral cells line

To support the chemical evidence, a biological screening of all the compounds was performed through MTT assays, which allowed the testing of numerous experimental conditions simultaneously to assess the best compounds, concentrations, and treatment times. First, the anticancer activity of these new σ/HDACi dual-ligands was screened, exposing a human gastric adenocarcinoma cell line (AGS) to 0.1, 1, and 10 μM of all the synthetized compounds for 24, 48, and 72 h. AGS is a solid gastric cancer whose pathogenesis and malignancy are strictly dependent on HDAC activity. In particular, more than one isoforms (1, 2, 3, 6) seems to be involved in gastric cancer development[41], which appears to be strongly influenced by epigenetic factors [42]. For most compounds (Fig. S1), no significant changes or more remarkable differences were observed compared to the control sample, while cells treated with **6** at highest concentrations appeared to have a considerable reduction in viability at all the experimental times (Fig. S1A). Even though, to a lesser extent, the same happened to **9a**-treated AGS cells at the highest concentration after 48 and 72 h (Fig. S1A). As for **9b**, the reduction in cell viability was present at all the experimental times in cells treated with the concentration of 10 μM (Fig. S1B). For these reasons, compounds **6**, **9a**, and **9b** were chosen for further analyses.

Three additional tumor cell lines, namely human colorectal carcinoma (HTC116), human breast cancer (MCF7), and human prostate adenocarcinoma (PC3), with different expressions of σ_1R, σ_2R, and of the HDAC enzyme isoforms, were then selected to test further the anticancer potential of the three most promising compounds (**6**, **9a**, and **9b**). AGS cells were also included in this set of experiments since six different concentrations were tested, ranging from 0 to 80 μM (Figs. S2–S4), and the IC_{50} was calculated for each compound (Table 2). The concentration range was chosen according to data already present in the literature and the results obtained in the previous experiments. Being the selected compounds already effective at lower concentrations, it was decided that an eight-fold increase in the concentrations could be enough to have a good dose–response curve. The viability of all the cell lines appeared strongly reduced by the exposure to compounds **6** (Fig. S2) and **9b** (Fig S4), whereas the compound **9a** (Fig. S3) shows milder cytotoxic effects, especially against the breast and prostate cancer cell lines, namely MCF7 and PC3. Compound **9a** showed a good IC_{50} on AGS and HCT116, whereas both **6** and **9b** had an IC_{50} lower than 10 μM for all the cell lines. In particular, **6** showed an IC_{50} of 0.87 μM on HCT116 cells, the lowest IC_{50} observed in our experimental study (Table 2). These results suggest the involvement of the σ1 receptor, for which the compounds **6** and **9b** have high affinity, in the anticancer effects exerted by the compounds. Indeed, σ_1R was crucial for colorectal cancer malignance [43] and prostate cancer target therapy [44]. The MCF-7 cells, which show a very low σ_1R expression [45], are still affected, and **9a**, which has no affinity for either the two σ receptors, retains some cytotoxic activity. These two findings conclude that binding to the σ receptors is not the only mechanism at the basis of the antiproliferative effect exerted by our compounds.

Therefore, being our molecules designed to have also an HDAC inhibitory activity, the viability of the same four cell lines was evaluated in the presence of the well-known HDACi valproic acid (VPA) and of the σ_1 antagonist BD1063, alone or in combination, and compared with the effects of compounds **6**, **9a**, and **9b**. VPA and BD1063, alone or in combination, showed a slight decrease in cell viability only at the highest dose of 80 μM in AGS (Fig. 3) and HCT116 cells (Fig. 4), while in MCF7 breast cancer (Fig. 5), cytotoxicity for BD1063 was found at the lowest doses of 1 and 5 μM. However, it was not confirmed at other doses except for 80 μM. As for PC3 prostate cancer cells (Fig. 6), the effects were diverse, but the cytotoxicity ascribable to VPA and BD1063 was never comparable to the one exerted by compounds **6**, **9a**, and **9b** in the same experimental conditions. These results are unsurprising since VPA acts as an HDAC class I inhibitor at higher doses than the ones used in our experimental system, even in the same cell lines considered for our study [46,47]. Such results confirm that the chemical combination of HDAC inhibitors and a σ receptor antagonists is a successful strategy to improve the antiproliferative properties of the compounds.

However, since the HDAC family comprehends many isoforms, divided per classes, and their expression and role can vary even among different cell lines of the same tumor type, the next step was the assessment of the ability of compounds **6**, **9a**, and **9b** to inhibit the pan-HDAC activity in the same cell lines used for viability assays (Fig. 7). Interestingly, an inhibition of the HDAC activity higher than 50% was observed in the cell lysates from all the four different cancer cell lines, when exposed to all the three chosen compounds. In particular, compound **6** appears to have an ability to inhibit histone deacetylase activity comparable to the reference compound Trichostatin A (TSA). Indeed, the calculation of IC_{50} results in an IC_{50} of 0.59 μM for compound **6**. In addition, compound **9a** also showed a low IC_{50} of 1.01 μM, while the HDAC inhibition was moderate for compound **9b** with an IC_{50} of 12.45 μM (Table 2 and Fig. S5). Looking at these results and the cell viability findings, it can be suggested that compound **6** has the best biological activity because of its good affinity for σ_1R and its low IC_{50} for HDAC enzymes. The conclusion is also supported by the successful use of the same strategy in other types of cancer [47]. It is worth noting that the compound **9a**, which has no affinity for the sigma receptors, fails to exert a cytotoxic effect at values comparable to those of the other two compounds when administered to breast and prostate cancers, suggesting the action on these cell lines goes mainly through the binding of sigma receptors [48].

On the other hand, compound **9a** retains activity against the two cell lines from the digestive tract despite having no affinity for sigma receptors, suggesting that the antiproliferative effect is due to HDAC inhibition. Speculating which HDAC isoforms can be the targets of our compounds is not easy, and our findings will require further investigation focused on this aspect, as well as on the molecular mechanisms at the basis of the antitumoral effects of our best compounds.

Finally, since this study aims to synthesize dual ligands with promising antitumoral activity and considering the results of the biological assays, compounds **6** and **9b** were chosen as the best candidates. Despite the better HDAC inhibitory activity and antiproliferative effect compared to **9b**, compound **9a** was discarded due to the extremely weak affinity to both σR. The effects of the best dual-ligands **6** and **9b** were explored on the normal human keratinocyte cell line HaCaT to assess their selectivity. The human keratinocyte cells were treated with different concentrations of the two compounds ranging from 0 to 80 μM (Fig. 8). Compound **9b** seemed to have cytotoxicity on a normal cell line comparable to that exerted on cancer cells. On the other hand, compound **6**, which showed an IC_{50} lower than 5 μM for HCT116 and AGS, appeared to not be very toxic for HaCaT cells at the same concentration.

Table 2
IC_{50} values obtained with MTT assay and Inhibitory activity against HDACs of dual-ligand compounds.

	IC_{50} [μM] ± SD[a]				IC_{50} [μM][b]
Compd	AGS	HCT116	MCF7	PC3	HDACs
6	3.5 ± 1.29	0.9 ± 0.16	8.4 ± 4.78	7.5 ± 3.09	0.59
9a	8.2 ± 0.86	2.9 ± 1.79	15.0 ± 8.09	26.8 ± 3.73	1.01
9b	2.9 ± 2.32	3.4 ± 4.22	8.8 ± 0.30	5.8 ± 2.84	12.45

[a] Each value is the mean ± SD of at least three experiments performed in triplicate. [b]HCT116 cell lysate was used as a source of HDAC activity (see Fig. S5 for a graphical representation).

2.5. Stability profile

In vitro, hydrolysis studies of selected compounds were performed at 37 °C in simulated gastric fluid (hydrochloric acid buffer, pH 1.3), phosphate buffer (pH 7.4), and human plasma using HPLC with UV detection (Table 3) [49]. All the tested compounds were more stable in

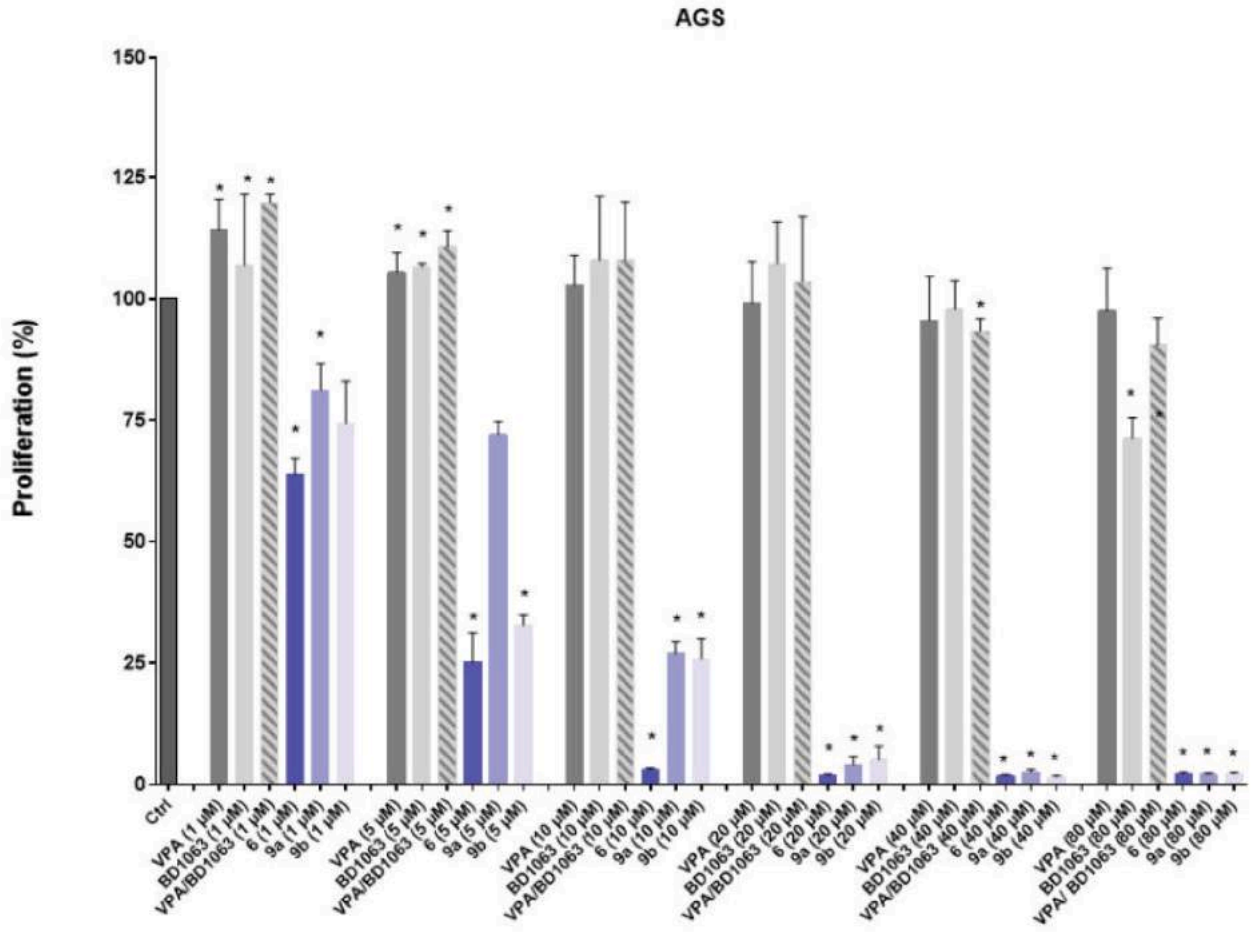

Fig. 3. Antiproliferative effects on AGS cells of **6**, **9a**, and **9b**, the HDACi valproic acid (VPA), and the σ_1 antagonist BD1063 (range from 1 to 80 μM, considering the calculated IC_{50} values). The latter two were administered alone or in combination. Ctrl, untreated cells. Data represent % of proliferation with respect to the control. *, $p < 0,05$ *vs.* Ctrl.

phosphate buffer (pH 7.4) than in hydrochloric acid buffer (pH 1.3). Compound **9a** was the least stable compound showing $t_{1/2}$ higher than 26 h, which, in any case, would guarantee the achievement of the active site after oral administration without undergoing degradation. The observed acid stability of the compounds mentioned above was essential for oral administration. Moreover, no appreciable differences were detected among the compounds with respect to their susceptibility to enzymatic hydrolysis in human plasma. They resulted stable ($t_{1/2} > 40$ h) in human plasma at 37 °C, suggesting that enzymes, such as plasma esterases or proteases, did not affect their stability. The increased stability of the amide linkages, along with the bulkiness of these compounds, probably, interfered with their ability to bind to the enzymes' active sites, making them not easily accessible.

2.6. *In silico ADME profile*

Absorption, distribution, metabolism, and excretion (ADME) properties are critical parameters in drug development. Recently, in silico models were developed to predict and optimize ADME properties of drugs at the early stages of their development [50]. In this study, ADME compounds' profiles were calculated using the Swiss ADME online software. This study was conducted to obtain information on the pharmacokinetic characteristics of selected compounds. All the predicted parameters explained the drug-likeness and improved ADME properties of synthesized ligands. As shown in Table 4, all compounds had passed Lipinski's rule of five as displaying zero violation. Lipinski's rule of five was used to detect the drug-likeness of the synthetized derivatives. According to this rule, the features a drug should have to be orally active are molecular weight (<500 g/mol), Log P (<5), H-bond donor (<5), and H-bond acceptor (<5). The results indicated that compounds **9a** and **9b** were moderately water-soluble, while compound **6** was quite soluble. The ability to cross the biological membranes, such as the blood–brain barrier (BBB) and the gastrointestinal (GI) tract was confirmed by the in-silico distribution parameters. Notably, the BBB permeability values suggested that all compounds showing reasonable lipophilia (cLogP about 3) could easily penetrate the central nervous system. Moreover, these ligands also presented high gastrointestinal absorption due to their favorable physicochemical properties. On the other hand, skin permeability for all ligands was scarce (Log K_p about –6 cm/s).

Cytochrome P450 enzymes, located in the liver and intestine, represent a class of enzymes mainly involved in drugs' metabolism. Drugs can inhibit or induce them, resulting in drug interactions that can lead to toxicity or decrease pharmacological effects. Prediction of inhibition of the main cytochromes was calculated with SwissADME in a binary form (yes/no).

For metabolism parameters, the results obtained with the SwissADME program indicated that none of all tested ligands had potential as an inhibitor of cytochrome CYP2C9 but as CYP2D6 inhibitors. CYP3A4, endowed with low substrate specificity, is the most abundant enzyme among the CYP3A subfamily. Compounds **9a** and **9b** could act as cytochrome CYP3A4 inhibitors with respect to compound **6.** Compound **9a** was also predicted to be a cytochrome CYP1A2 inhibitor compared to

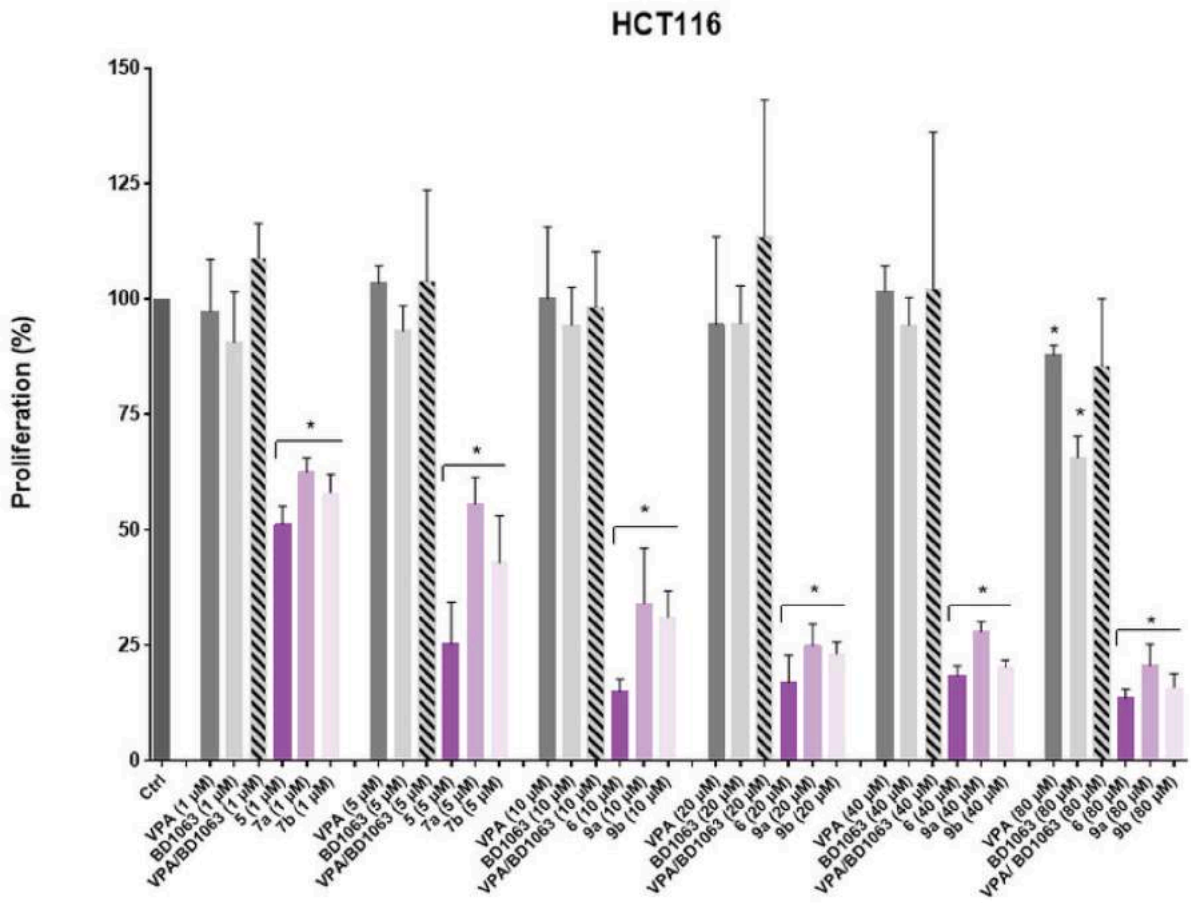

Fig. 4. Antiproliferative effects on HCT116 cells of **6**, **9a**, and **9b**, the HDACi valproic acid (VPA), and the σ_1 antagonist BD1063 (range from 1 to 80 μM, considering the calculated IC_{50} values). The latter two were administered alone or in combination. Ctrl, untreated cells. Data represent % of proliferation with respect to the control. *, $p < 0,05$ *vs.* Ctrl.

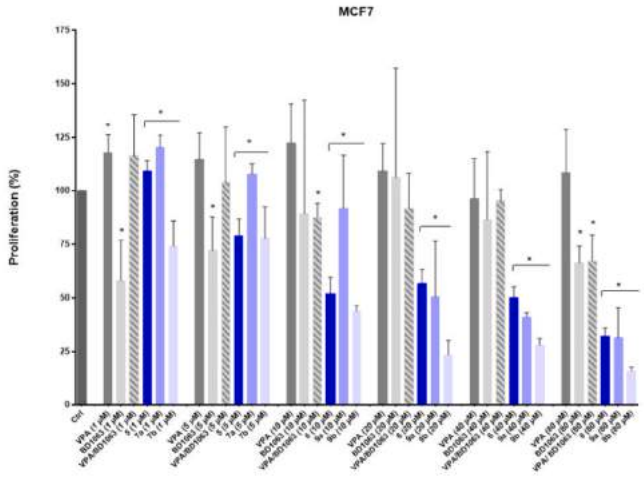

Fig. 5. Antiproliferative effects on MCF7 cells of **6**, **9a**, and **9b**, the HDACi valproic acid (VPA), and the σ_1 antagonist BD1063 (range from 1 to 80 μM, considering the calculated IC_{50} values). The latter two were administered alone or in combination. Ctrl, untreated cells. Data represent % of proliferation with respect to the control. *, $p < 0,05$ *vs.* Ctrl.

other test ligands. On the other hand, only compound **9b** was predicted to be a cytochrome CYP2C19 inhibitor, which is involved in detoxifying potential carcinogens or the bioactivation of various environmental procarcinogens. Thus, compounds **9a** and **9b** had the most chance as cytochrome inhibitors with three types of cytochromes.

2.7. Molecular modeling studies

Molecular modeling studies [51,52] supported the mechanism of recognizing the most active compounds within the σ_1 and σ_2 receptors and HDACs binding pockets. The two best compounds were subjected to docking studies using AutoDock Vina as implemented in the YASARA software to evaluate the established interactions with the σ_1 and σ_2 receptors. The docking studies were performed on all the protonation states of the compounds at pH 7.4, previously calculated using the Marvin software [53,54]. The calculated free energies of binding (ΔG) and the calculated and experimental K_i values at the binding site of the σ_1 and σ_2 receptors are reported in Table S1, with the respective 2D structures for all the protonation states.

From the data reported in Table S1, the in-silico calculated binding constants were in good agreement with the experimental data. By examining the most active compound at the σ_1 receptor (compound **6**, $K_i = 38.28$ nM), we can see that both protonation states (1 and 2) had a comparable constant of binding (Table S1). In fact, analyzing the two poses inside the receptor site (Figs. 9 and S6), we noted the presence, in both cases, of the salt bridge with the E172 residue. The structure with the most active protonation state ($\Delta G = -10.36$, **6**–**1**) among the various

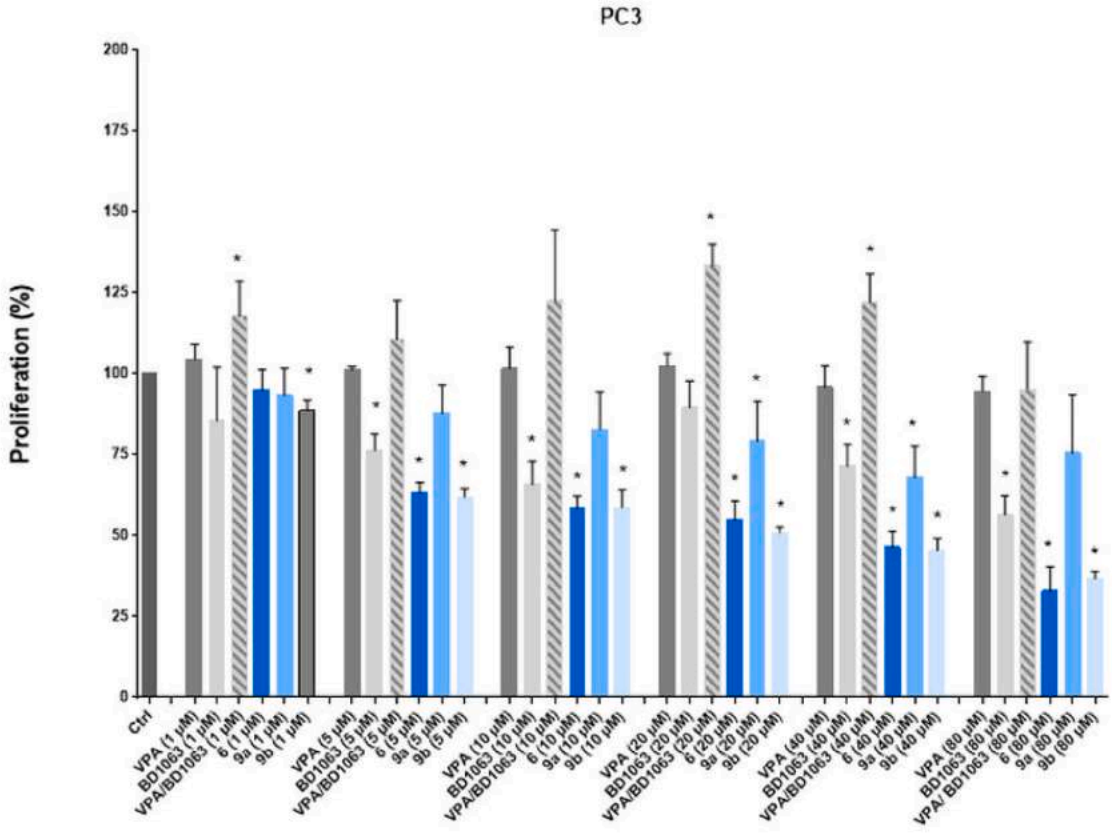

Fig. 6. Antiproliferative effects on PC3 cells of **6**, **9a**, and **9b**, the HDACi valproic acid (VPA), and the σ_1 antagonist BD1063 (range from 1 to 80 μM, considering the calculated IC_{50} values). The latter two were administered alone or in combination. Ctrl, untreated cells. Data represent % of proliferation with respect to the control. *, $p < 0,05$ *vs.* Ctrl.

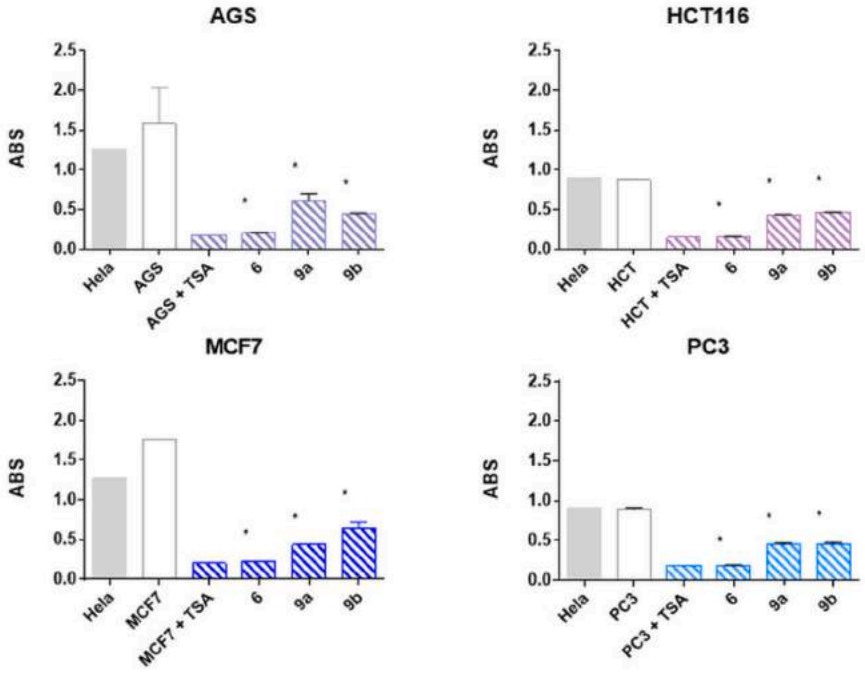

Fig. 7. Evaluation of IC_{50} on HDAC activity by compounds **6**, **9a**, and **9b**. Positive ctrl, HeLA nuclear extract. Ctrl, untreated cellular extract. ABS, absorbance. *, $p < 0,05$ *vs.* Ctrl.

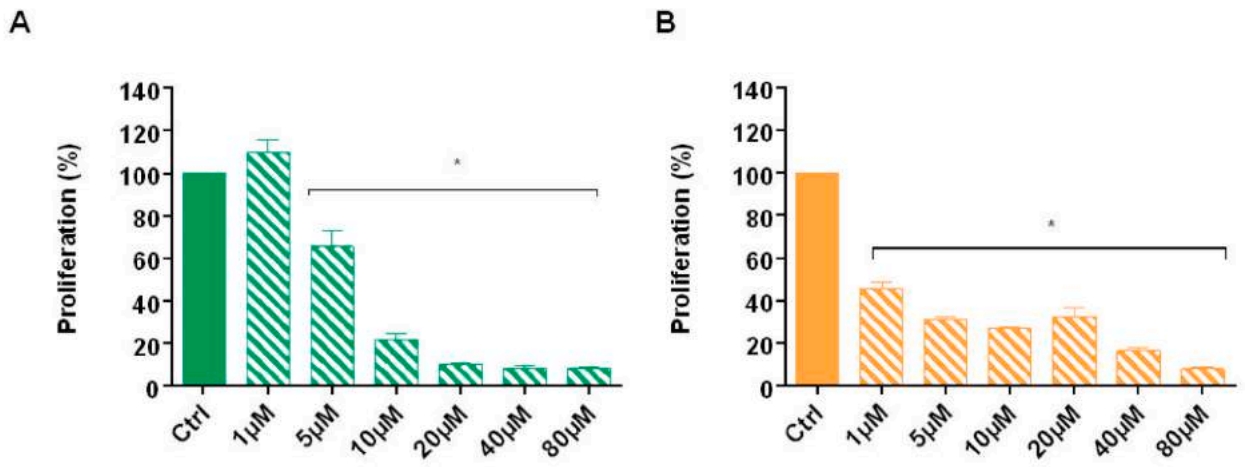

Fig. 8. Antiproliferative effects of **6** (A) and **9b** (B) from 0 to 80 μM on the human keratinocyte cell line HaCaT. Ctrl, untreated cells. Data represent % of proliferation with respect to the control. *, $p < 0,05$ *vs.* Ctrl.

Table 3
Stability studies[a].

	6		**9a**		**9b**	
	$t_{1/2}$ (h)	$K_{obs}^{(h-1)}$	$t_{1/2}$ (h)	$K_{obs}^{(h-1)}$	$t_{1/2}$ (h)	$K_{obs}^{(h-1)}$
pH 1.3	stable	—	26.7 (±0.35)	0.026 (±0.002)	42.4 (±0.31)	0.016 (±0.004)
pH 7.4	51.3 (±0.26)	0.014 (±0.005)	stable	—	stable	—
Human plasma	40.09 (±0.47)	0.017 (±0.09)	44.67 (±0.21)	0.016 (0.013)	stable	—

[a] Values are means of three experiments.

Table 4
ADME profile of selected compounds using SwissADME software.

Compound	Solubility	cLog P	BBB permeability	GI absorption	Skin permeability	Lipinski's rule
6	Soluble	2.17	Yes	High	–6.82 cm/s	0 violations
9a	Moderate	3.08	Yes	High	–6.46 cm/s	0 violations
9b	Moderate	3.64	Yes	High	–6.07 cm/s	0 violations

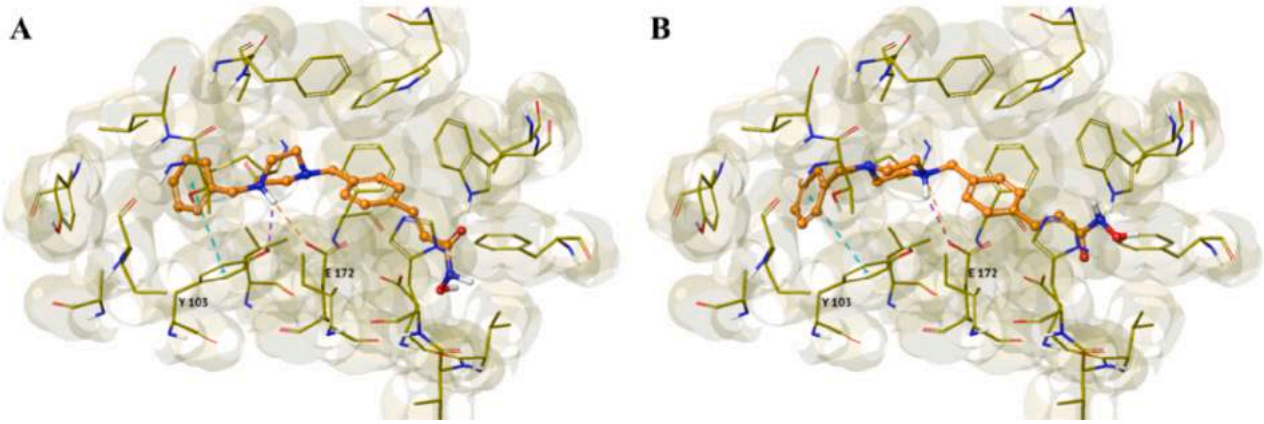

Fig. 9. Compound **6**–**1** (A) and **6**–**2** (B) in 3D representation. Protein is shown as an olive-green surface, while residues, involved in the most critical interactions, are depicted as olive-green thin tubes. The ligand is represented as orange balls and sticks. H-bonds, salt bridge, and π-π interactions are indicated as violet, orange, and cyan dashed lines, respectively.

interactions establishes some more significant ones: a hydrogen bond and a π-π interaction with the Y103 residue.

Among the various protonation states of compound **9b**, the most active were those in which nitrogen bound to methyl was protonated. Protonation in this nitrogen leads to the formation of two stereoisomers, among which the stereoisomer *R* was more active ($\Delta G = -9.63$, Table S1). The *R* enantiomer established salt bridges with E172 and D126, a π-cation interaction with F107, and π-π interactions with Y103, H154, and F133 (Fig. 10 and S7).

In order to shed light on the high potency of compounds **6** and **9b** in inhibiting HDACs, molecular docking simulations were carried out to figure out their possible binding mode with HDACs using AutoDock

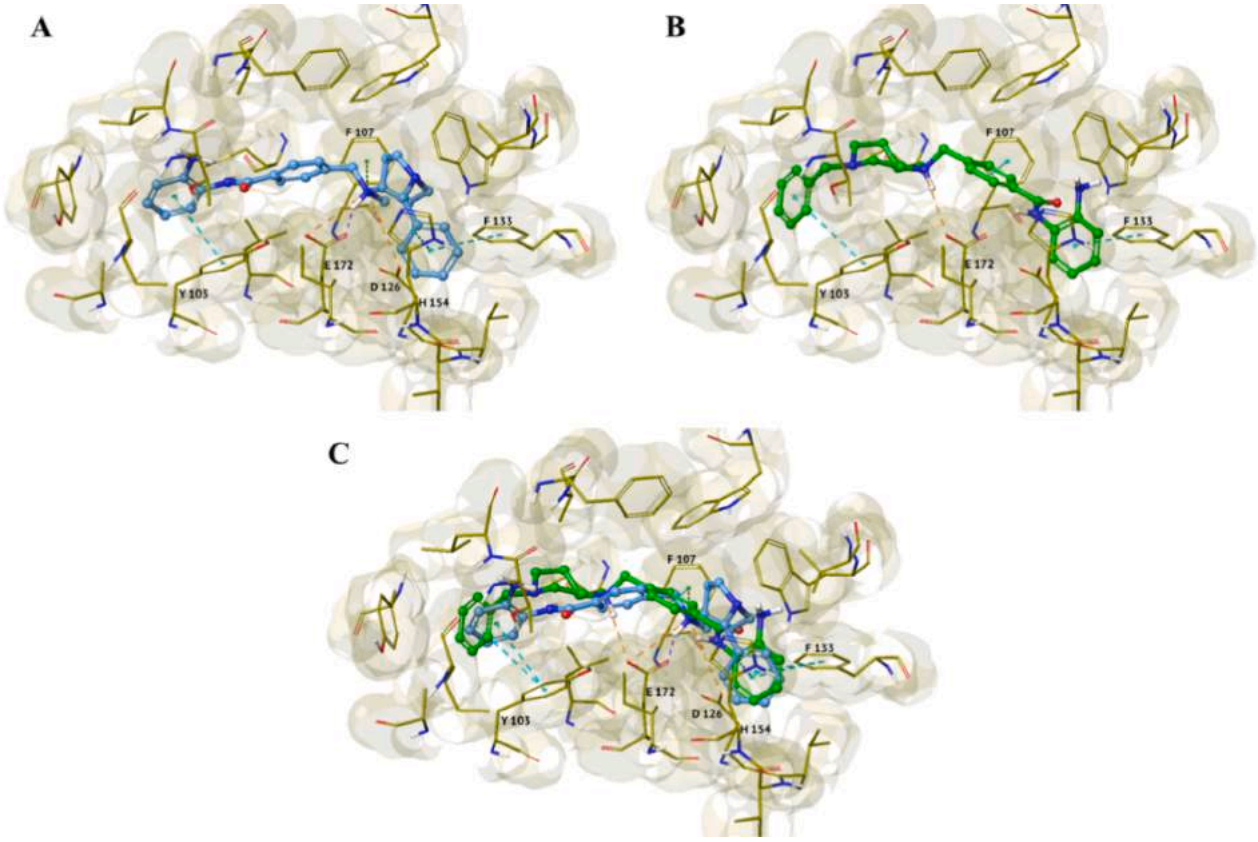

Fig. 10. Compound **9b-2**(*R*) (A), **9b-2**(*S*) (B), and **9b-2**(*R*) and (*S*) (C). Protein is shown as an olive-green surface, while residues, involved in the most important interactions, are depicted as olive-green thin tubes. The ligand is represented as azure balls and sticks. H-bonds, salt bridge, π-cation, and π-π interactions are indicated as violet, orange, green, and cyan dashed lines, respectively.

Vina. Following our experience [55], the docking protocol was validated by re-docking the co-crystalized ligands in the HDACs 3D structures, except in the isoforms 1 and 3 that exhibit only models of the unbound state in the PDB. The RMSD value (Table S4) for four PDB models was <2 Å, indicating the docking results' confidence. However, the RMSD of 2.5 Å, observed for the HDAC2 co-crystallized ligand, can be explained by its high flexibility. In particular, a good overlap of the benzamide fraction responsible for the Zn^{2+} coordination was observed, while the increase in the RMSD value can be related to the cap portion. For compounds **6** and **9b**, we docked all the physiological protonation states (Table S3), also considering the stereochemistry of the protonated chiral nitrogen. Moreover, TSA, a pan-HDAC inhibitor, was included as a positive control in the docking simulations. The binding energy values of both compounds docked into the active site of HDACs isoforms, considering all their protonation states, are shown in Table S5. The docking results (Table S5) indicated that compound **6**, with ΔG values better than or very similar to TSA, exhibited a pan-HDACs inhibitory behavior, characteristic of most hydroxamic acid-based HDAC inhibitors [56]. Conversely, compound **9b** reached the catalytic site of HDAC1, HDAC2, HDAC3, and HDAC8, behaving as a selective inhibitor for class I, as generally shown by compounds with an amino-benzamide motif [57]. Interestingly, in all HDAC binding pockets, the protonation states of compound **6** exhibited ΔG values very close among them, within an energetic window of 3 kcal/mol. This evidence indicated that the compound in all protonation forms could bind to the receptor without particular changes in affinity. Regarding compound **9b**, we observed a similar behavior of all its protonation states only for the active site of HDAC1, HDAC2, and HDAC3. Instead, in the HDAC8 binding site, the protonation states of **9b** with a single positive charge exhibited a better affinity than the others. In particular, the structure with a single positive charge on the nitrogen of the piperidine showed the best affinity towards this target. Firstly, to analyze the binding mode of our compounds, we calculated the distance of hydroxamic and benzamide groups from the Zn^{2+} ion for **6** and **9b**, respectively (Tables S4,5), to evaluate the coordination geometry. For compound **6**, monodentate chelation was observed in all generated docking poses. Conversely, compound **9b** with its benzamide portion showed a bidentate interaction with the catalytic Zn^{2+} of HDAC1, HDAC2, and HDAC3, thus explaining its good affinity towards these targets. In the binding pocket of the HDAC8, only the **9b** protonation state with the lowest probability of existence was able to establish bidentate interactions with the Zn^{2+} ion, while monodentate chelation characterizes the other species. On the other hand, the lower affinity exhibited by **9b** towards the isoforms 6 and 7 can be related to the absence of Zn^{2+} chelation, with distances >10 Å also suggesting a ligand position of the ligand far from the catalytic tunnel. Then, we analyzed the molecular interactions between our ligands and all HDAC binding pockets (Tables S6–8), considering the different protonation states used in this work. Regarding compound **9b**, its selectivity towards HDACs class I can be explained by the observation that docking simulations always placed its protonation states outside the catalytic tunnel of the isoforms 6 and 7. Moreover, in all the **9b** poses generated for the HDAC4 binding pocket, the observation of harmful interactions explains its lower affinity. Apart from the coordination involving the ZBG (zinc-binding group), the key interactions for compound **6** binding appeared to be several stacking interactions, established by its central aromatic scaffold and electrostatic ones, such as H-bonds, π-cation, and salt-bridges. To describe the most important interactions of **6** and **9b** within the binding site of the different HDACs, we focused on the best docking poses of their most probable protonation state (Figs. 11–13). For the HDACs class I, both compounds showed good interactions with similar binding modes, especially for the ZBG and the central aromatic core (Figs. 11 and 12). The HDAC1 key residues involved in the main

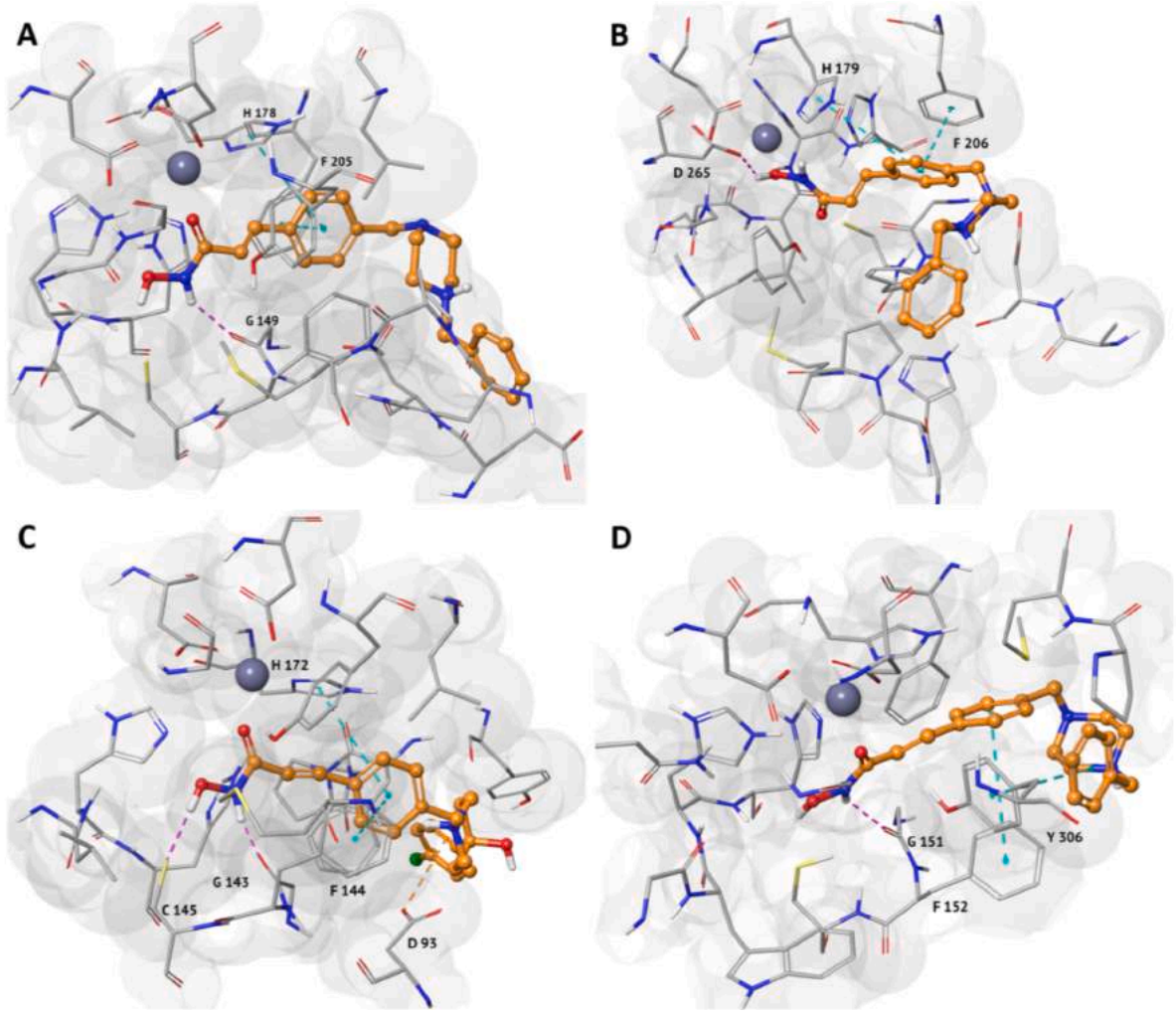

Fig. 11. Best docking poses of compound **6** with HDACs class I. Best docked poses of the most probable protonation state of **6** with the crystal structure of (A) HDAC1, (B) HDAC2, (C) HDAC3, and (D) HDAC8. Protein is shown as a grey surface, while the residues involved in the most critical interactions are depicted as a thin gray tube. The ligand is represented as orange balls and sticks. H-bonds, salt bridge, and π-π interactions are indicated as violet, orange, and cyan dashed lines, respectively.

interactions with both compounds are G149, H178, and F205 (Figs. 11A and 12A). Specifically, G149 was involved in an H-bond acceptor through its carbonyl group with the hydroxamic acid and amide moiety of compounds **6** and **9b**, respectively. H178 established a π-π interaction and an H-bond acceptor with the **6** styrene ring and the **9b** aniline group, respectively. Instead, a π-π and π-cation interactions were observed between F205 and the central aromatic portion of both ligands. Moreover, both enantiomers of compound **9b** shared a salt bridge between their aliphatic ammonium group and the side chain of D99. In the HDAC2, both ligands shared a similar binding mode with the ZBG placed in the catalytic cavity and the central aromatic portion interacting with the residues of the catalytic tunnel, which displayed a lipophilic behavior, such as F206, F151, and H29 (Figs. 11B and 12B). In particular, compound **6** established an H-bond donator between its hydroxamic group and the side chain of D265, while two π-π interactions were formed between its styrene ring and the side chains of H179 and F206. The binding mode of both **9b** enantiomers was characterized by a π-π interaction with the side chain of F151 and by two H-bonds donors, involving their aniline and amide portions with the side chain of D177 and the backbone of G150, respectively.

Conversely, the stacking interaction between the benzylic group of compound **9b** and the side chain of H29 was observed only in the docking pose of the *S* enantiomer, explaining its better affinity towards the target than the *R* enantiomer. Regarding the complexes with the HDAC3 (Figs. 11C and 12C), our ligands share the key residues involved in different interactions, such as G143, H172, F144, and D93. As for G149 in the HDAC1 binding pocket, G143 is involved in an H-bond acceptor through its carbonyl group with the hydroxamic acid and amide moiety of compounds **6** and **9b**, respectively. The side chains of H172 and F144 establish π-π interactions with the central aromatic portion of both ligands, while D93 forms a salt bridge with the positively charged nitrogen. Moreover, in the binding mode of compound **9b**, the benzamide portion established more H-bonds than the hydroxamic moiety of compound **6**. In the binding pocket of the HDAC8 (Figs. 11D and 12D), only an H-bond with the backbone of G151 was observed, while hydrophobic and π-π interactions have to be considered the most important for target affinity. In particular, the key residues involved in the latter interactions are F152 and Y306. Finally, we observed that compound **6** well also fits the binding pockets of the class IIa and IIb HDACs (Fig. 13). In particular, the H-bond established by its hydroxamic moiety with G811 and several hydrophobic interactions were pointed out as the key interactions in its complex with the HDAC4 (Fig. 13A). In the HDAC7 cavity, compound **6** was able to interact with the target through an H-bond with G678, three π-π interactions between its aromatic portions and the side chain of H709 and F738, and a salt-bridge involving its ammonium group and the side chain of D626 (Fig. 13B).

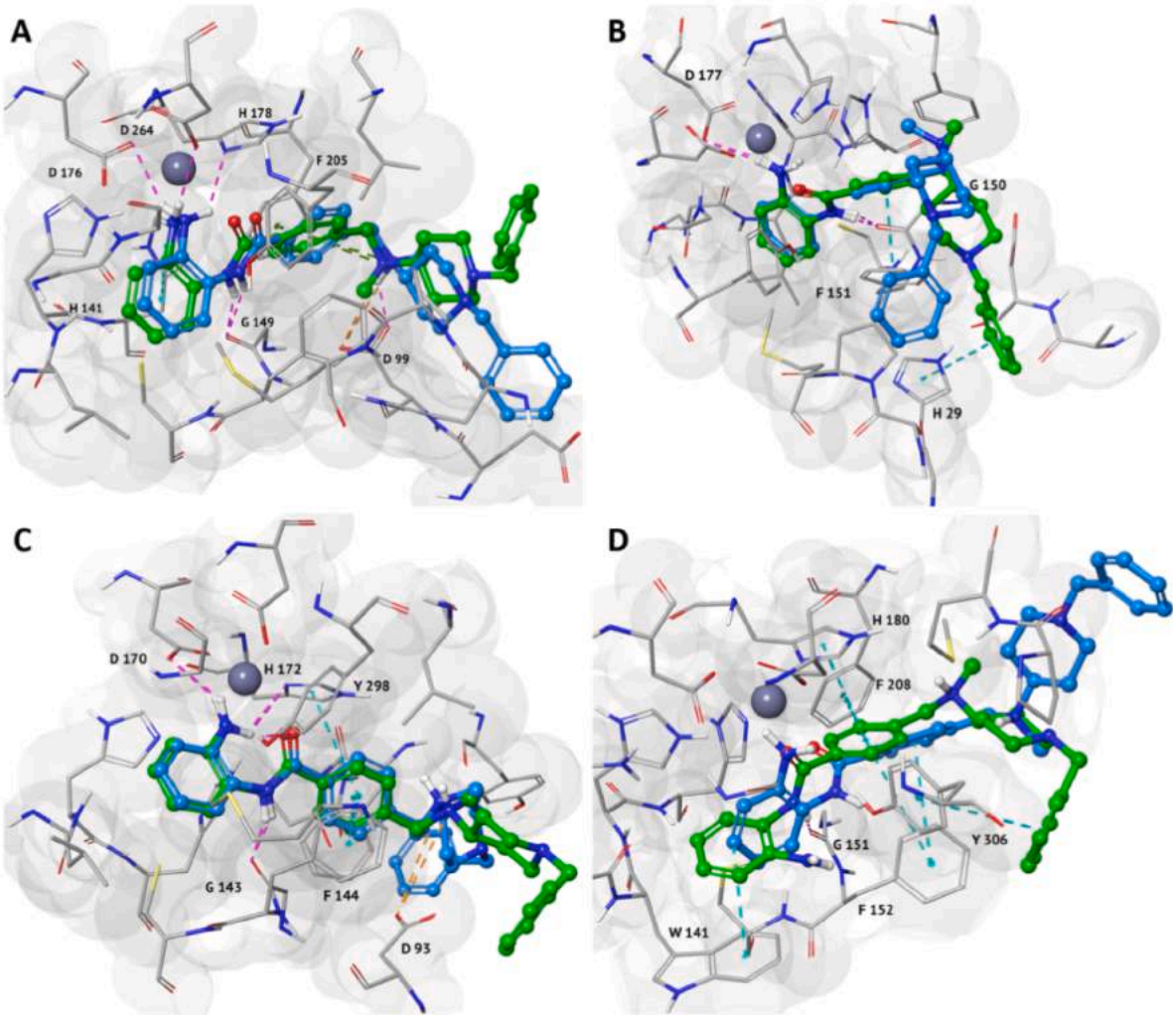

Fig. 12. Best docked poses for both enantiomers of compound **9b** with HDACs class I. Best docked poses of both enantiomers of the most probable protonation state of **9b** with the crystal structure of (A) HDAC1, (B) HDAC2, (C) HDAC3, and (D) HDAC8.The protein is shown as a grey surface, while residues involved in the most critical interactions are depicted as thin gray tubes. Enantiomers *R* and *S* of ligand were represented as azure and green, respectively, balls and sticks. H-bonds, salt bridge, π-cation, and π-π interactions are indicated as violet, orange, green, and cyan dashed lines, respectively.

Instead, compound **6** interacted with the HDAC6 through different hydrophobic contacts and four H-bonds, which involved the side chain of G619, C621, and Y782 and the backbone of H610 (Fig. 13C). Conversely, compound **9b** didn't well match the class IIa and IIb HDACs' binding pocket explaining its selectivity towards HDAC class I. Specifically, it showed in the HDAC4 binding pocket several harmful interactions due to steric hindrance occurring with the benzamide portion, while in the complexes with the isoforms 6 and 7, it was even positioned outside the catalytic cavity (data not shown).

3. Conclusions

This work represents a challenge in discovering new, safer, and more efficient drugs than single-target drugs. Taking advantage of the multitarget approach, we proposed, for the first time, dual σR/HDACi ligands able to bind the σ1 receptor and inhibit the HDAC enzyme at once, looking to balance their activity between the two targets.

Screening on several cancer cell lines identified multiple opportunities for the different potential employment of the designed dual-ligands as a possible way to treat different cancer types. Notably, compound **6** ($K_i\sigma_1R = 38 \pm 3.7$, $K_i\sigma_2R = 2917 \pm 769$) strongly reduced the viability of the tumor cells from different regions of the digestive tract, namely AGS and HCT116, as well as compound **9b** ($K_i\sigma_1R = 52 \pm 3.9$ nM, $K_i\sigma_2R = 1588 \pm 233$) did, although to a lesser extent; on the other hand, compound **9a** ($K_i\sigma_1R = 3758 \pm 929$ nM, $K_i\sigma_2R > 10000$ nM) exhibited a good antiproliferative activity only against HCT116. Moreover, their toxicity was assessed on human keratinocyte cells HaCaT, showing that compound **6** appeared to be the least toxic drug.

Specific molecular docking studies confirmed the experimental data. In particular, compound **6** showed a comparable σR binding constant for both protonation states due to the presence of the salt bridge with the E172 residue in both cases and exhibited monodentate chelation of the catalytic Zn^{2+} in all generated docking poses, suggesting a pan-HDACs inhibitory behavior very similar to the TSA pan-HDAC inhibitor. Conversely, compound **9b** was more active when the nitrogen bound to methyl was protonated to do the stereoisomer *R*, establishing salt bridges with E172 and D126, and compound **9b** exerted a selective inhibition for class I, reaching the catalytic site of HDAC1, HDAC2, HDAC3, and HDAC8. In fact, the benzamide portion showed a bidentate interaction with HDAC1, HDAC2, and HDAC3 catalytic sites.

Altogether, these results suggested that compound **6** could be the best candidate for treating complex diseases like cancer, which regulates two different targets equally through the innovative multitarget approach, even though further studies about the specific mechanism should be carried out and should not be excluded.

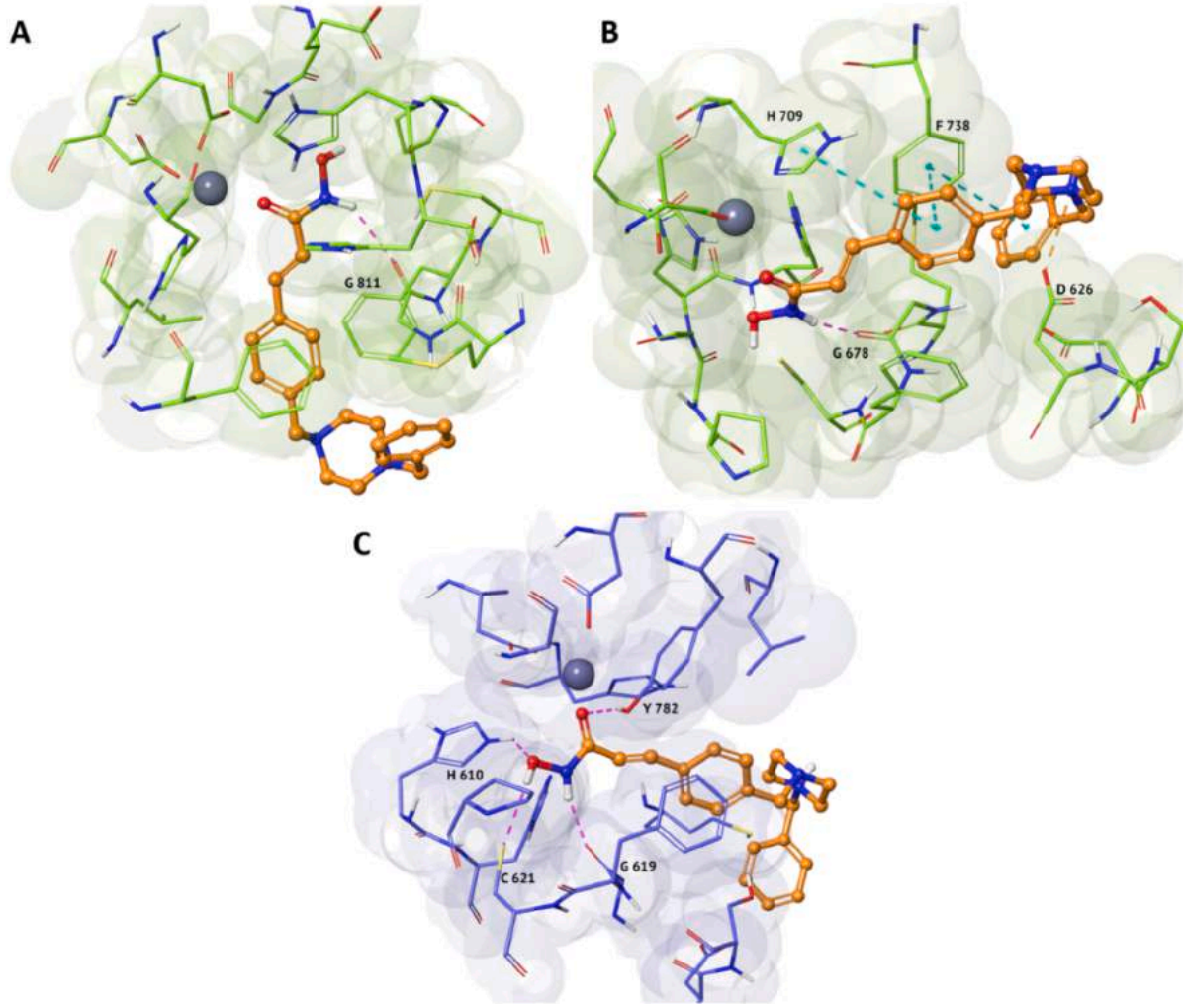

Fig. 13. Best docking poses of compound **6** with HDACs class IIa and IIb. Best docked poses of the most probable protonation state of **6** with the crystal structure of (A) HDAC4, (B) HDAC7, and (C) HDAC6. Proteins are shown in a yellow-green and faded blue surface for class IIa and IIb, respectively, while residues involved in the most critical interactions are depicted as yellow-green and faded thin blue tubes, respectively. The ligand is represented as orange balls and sticks. H-bonds, salt bridge, and π-π interactions are indicated as violet, orange, and cyan dashed lines, respectively.

4. Experimental section

4.1. Chemistry

4.1.1. General remarks

Reagent-grade chemicals were purchased from Sigma-Aldrich (St. Louis, MO, USA) or TCI (Tokyo, Japan) and were used without further purification. All reactions involving air-sensitive reagents were performed under N_2 in oven-dried glassware using the syringe-septum cap technique. All reactions were monitored by thin-layer chromatography (TLC), performed on silica gel Merck 60 F254 plates; the spots were visualized by UV light (λ = 254 and 366 nm) and iodine chamber. Melting points were determined on a Büchi B-450 apparatus in capillary glass tubes and are uncorrected. Flash chromatography purification was performed on a Merck silica gel 60, 0.040–0.063 mm (230–400 mesh), stationary phase using glass columns with a diameter between 1 and 4 cm. Nuclear magnetic resonance spectra (^{1}H NMR and ^{13}C NMR recorded at 500 MHz) were obtained on Varian INOVA spectrometers using $CDCl_3$, D_2O e DMSO-d_6 with a 0.03% of TMS as internal standard. Coupling constants (*J*) are reported in hertz. Signal multiplicities are characterized as s (singlet), d (doublet), t (triplet), q (quartet), m (multiplet), br (broad), app (apparent). Purities of all compounds were determined by microanalysis (C, H, N) that was performed on a Carlo Erba instrument model E1110; all the results agreed within ±0.4% of the theoretical values. The *Matrix Assisted Laser Desorption Time of Flight Mass Spectrometry* (MALDI TOF) analysis was performed using a 4800 MALDI TOF/TOF™ Analyzer (Applied Biosystem, Framingham, MA, USA). The instrument was equipped with an Nd:YAG laser (wavelength of 355 nm) of <500 ps pulse and 200 Hz repetition rate and working in positive-ion mode. The MALDI mass spectra of selected compounds were obtained in reflector mode. Samples were prepared by dissolving in THF the compounds (10 mg/mL) and the matrix *trans*-2-[3-(4-*tert*-butylphenyl)-2-methyl-2-propenyldene]malononitrile (0.1 mmol). Suitable volumes of matrix and compound solutions were mixed to obtain 1:1, 1:2, and 2:1 ratios (sample/matrix v/v). The mixture was deposited onto the MALDI sample holder and dried at room temperature for matrix crystallization.

4.1.2. General procedure for the synthesis of methyl (E)-3-[4-(4-benzylpiperazin-1-yl)phenyl]acrylate (**3**)

To a solution of 4-formylcinnamic acid (5.0 g; 28.4 mmol) in *N*,*N*-dimethylformamide anhydrous (DMF) was added K_2CO_3 (5.10 g; 37 mmol) and dropwise methyl iodide (5.68 g; 40 mmol) at room temperature and in a nitrogen atmosphere. The reaction mixture was stirred for 24 h at room temperature. Then, the solvent was evaporated under vacuum, the resulting residue treated with EtOAc, and washed saturated

solution of $NaHCO_3$. The organic and the aqueous phase were repeatedly separated, and the aqueous phase was extracted with EtOAc. The combined organics phases have been dried with anhydrous Na_2SO_4, filtered, and evaporated under vacuum to obtain 4.61 g of pure **2** (yield 85.4%). The obtained solid did not require any further purification. To a solution of 4-benzylpiperazine (1.26 mL; 7.3 mmol) in 10 mL of anhydrous tetrahydrofuran (THF) was added dropwise at room temperature and in nitrogen atmosphere compound **2** (1.4 g; 7.3 mmol) in 6 mL anhydrous THF. AcOH was added to the solution (0.420 mL, 7.3 mmol), and the reaction mixture was stirred for about 30 min and added dropwise to a $NaBH(OAc)_3$ solution (2.31 g; 10.9 mmol) in 1.85 mL of anhydrous THF at room temperature and nitrogen atmosphere. The reaction mixture was stirred overnight at room temperature. Subsequently, a saturated solution of $NaHCO_3$ was added, and the aqueous phase was repeatedly extracted with $CHCl_3$. The combined organic phases were dried with Na_2SO_4 anhydrous, filtered, and evaporated under vacuum. The crude was purified by MPLC using EtOAc as eluent to get 1.76 g of intermediate **3** (69% yield) as a white solid.mp 107–109 °C; ^{1}H NMR (500 MHz, D_2O): δ 3.46 (s, 8H, *H*-piperazine); 3.65 (s, 3H, COO*CH*$_3$); 4.31 (s, 4H, NC*H*$_2$); 6.43 (d, J = 5.0 Hz, 1H, CO*CH*); 7.34–7.56 (m, 9H + 1H, Ar*H* + ArC*H* = CH); ^{13}C NMR (125 MHz, D_2O): 50.48 (O*C*H$_3$), 50.53 (2*C*H$_2$-piperazine), 54.66 (2*C*H$_2$-piperazine), 62.30 (*C*H$_2$), 62.82 (*C*H$_2$), 121.24 (*C*H), 129.83 (*C*HAr), 131.34 (2*C*HAr), 131.79(2*C*HAr), 132.09 (2*C*HAr), 132.96 (2*C*HAr), 133.53 (*C-ipso*), 134.09 (*C-ipso*), 138.37 (*C-ipso*), 146.77 (*C*H), 171.86 (*C*O). Anal. calcd. for $C_{22}H_{26}N_2O_2$: C, 75.40; H, 7.48; N,7.99. Found: C, 75.36; H, 7.60; N, 7.74.

4.1.3. General procedure for the synthesis of methyl esters(**8a,b**)

To a solution of the specific ammine (1 mmol) and $NaHCO_3$ in absolute EtOH was added (1 mmol) dropwise intermediate **7** (1 mmol) at 50 °C and nitrogen atmosphere. The reaction mixture was stirred for 7 h at 50 °C and then stirred at room temperature overnight. Then the solvent was evaporated under vacuum, and the resulting residue was treated with EtOAc and washed with a saturated solution of $NaHCO_3$. The organic and the aqueous phases were repeatedly separated, and the aqueous phase was extracted with EtOAc and subsequently adjusted at pH 9 with Na_2CO_3. The aqueous phase was extracted with EtOAc, and the combined organics phases were dried with anhydrous Na_2SO_4, filtered, and evaporated under vacuum. The crude was purified by MPLC using EtOAc as eluent. According to this procedure, the following products have been obtained.

*4.1.3.1. Methyl 4-[(4-benzylpiperazin-1-yl)methyl]benzoate(**8a**).* White solid (86%): mp 82–83 °C; ^{1}H NMR (500 MHz, $CDCl_3$): δ 2.47 (s, 8H, *H*-piperazine), 3.51 (s, 2H, NC*H*$_2$), 3.54 (s, 2H, NC*H*$_2$), 3.89 (s, 3H, COOC*H*$_3$), 7.21–7.31 (m, 5H, Ar*H*), 7.38 (d, J = 9.0 Hz, 2H, Ar*H*), 7.96 (d, J = 9.0 Hz, 2H, Ar*H*); ^{13}C NMR (125 MHz, $CDCl_3$): 51.98 (O*C*H$_3$), 53.02 (2*C*H$_2$-piperazine), 53.13 (2*C*H$_2$-piperazine), 62.62 (*C*H$_2$), 63.01 (*C*H$_2$), 127.00 (*C*HAr), 128.16 (2*C*HAr), 128.92 (2*C*HAr), 129.18 (*C*HAr), 129.51 (*C*HAr), 129.83 (*C*HAr), 133.47 (*C*HAr), 138.04 (*C-ipso*), 140.34 (*C-ipso*), 143.81 (*C-ipso*), 167.03 (*C*O). Anal. calcd. for $C_{20}H_{24}N_2O_2$: C, 75.05, H, 7.46, N, 8.63. Found:C, 74.79, H, 7.79, N, 8.45.

*4.1.3.2. Methyl 4-{[(1-benzylpiperidin-4-yl)(methyl)amino]methyl}benzoate(**8b**).* White solid (49%): mp 240–242 °C; ^{1}H NMR (500 MHz, $CDCl_3$): δ 1.60–1.70 (m, 2H, *H*-piperidine), 1.73–1.79 (m, 2H, *H*-piperidine), 1.91–2.07 (m, 2H, *H*-piperidine), 2.18 (s, 3H, NC*H*$_3$), 2.37–2.46 (m, 1H, *H*-piperidine), 2.90–2.98 (m, 2H, *H*-piperidine), 3.48 (s, 2H, NC*H*$_2$), 3.61 (s, 2H, NC*H*$_2$), 3.89 (s, 3H, COOC*H*$_3$), 7.20–7.32 (m, 5H, Ar*H*), 7.38 (d, J = 8.0 Hz, 2H, Ar*H*), 7.96 (d, J = 8.0 Hz, 2H, Ar*H*); ^{13}C NMR (125 MHz, $CDCl_3$): 27.87 (*C*H$_3$), 37.85 (*C*H-piperidine), 51.91 (O*C*H$_3$), 53.23 (2*C*H$_2$-piperidine), 57.69 (2*C*H$_2$-piperidine), 61.04 (*C*H$_2$), 63.05 (*C*H$_2$), 126.89 (*C*HAr), 128.11 (2*C*HAr), 128.45 (2*C*HAr), 128.64 (2*C*HAr), 129.08 (2*C*HAr), 129.50 (*C-ipso*), 138.43 (*C-ipso*), 145.86 (*C-ipso*), 167.07 (*C*O). Anal. calcd. for $C_{22}H_{28}N_2O_2$: C, 62.25, H, 7.32, N, 6.50. Found: C, 62.12, H, 7.11, N, 6.59.

4.1.4. General procedure for the synthesis of N-(2-aminophenyl)amide (**4**, and **9a,b**)

To a solution of esters, **3**, **8a**, or **8b** (1 mmol) in MeOH, an aqueous solution of LiOH 1 M (2 mmol) was added dropwise at 50 °C. The reaction mixture was stirred at a temperature of 50 °C overnight. The solvent was evaporated under vacuum, the resulting residue dissolved in anhydrous DMF, and *o*-phenylenediamine (4 mmol) in DMF was added, followed by the addition of HOBt (3 mmol) and EDC (3 mmol). The reaction was stirred at room temperature for 24 h. Subsequently, EtOAc was added, and the organic phase was repeatedly washed with a saturated solution of $NaHCO_3$ and with a solution of NaCl. The combined organic phases were dried with anhydrous Na_2SO_4, filtered, and evaporated under vacuum. The crude was purified by MPLC using EtOAc as eluent. According to this procedure, the following products have been obtained.

*4.1.4.1. (E)-N-(2-aminophenyl)-3-{4-[(4-benzylpiperazin-1-yl)methyl] phenyl}acrylamide(**4**).* Beige solid (70%): mp 164–166 °C; ^{1}H NMR (500 MHz, $CDCl_3$): δ 2.49 (s, 8H, *H*-piperazine); 3.52 (s, 4H, NC*H*$_2$); 3.88 (br s, 2H, N*H*$_2$); 6.57 (d, J = 15.5 Hz, 1H, COC*H*); 6.77–6.84 (m, 2H, Ar*H*); 7.00–7.38 (m, 9H, Ar*H*); 7.4–7.5 (m, 2H, Ar*H*); 7.55 (br s, 1H, ArC*H* = CH); 7.71 (d, J = 9.0 Hz, 1H, Ar*H*); ^{13}C NMR (125 MHz, $CDCl_3$): 52.94 (2*C*H$_2$-piperazine), 52.99 (2*C*H$_2$-piperazine), 62.58 (*C*H$_2$), 62.95 (*C*H$_2$), 116.71 (*C*HAr), 118.20 (*C*H), 119.17 (*C*HAr), 119.54 (*C*HAr), 124.49 (*C*HAr), 125.09 (*C*HAr), 127.06 (*C*HAr), 127.86 (2*C*HAr), 128.18 (2*C*HAr), 129.23 (2*C*HAr), 129.57 (2*C*HAr), 133.47 (*C-ipso*), 137.83 (*C-ipso*), 140.34 (*C-ipso*), 140.71 (*C*NH$_2$), 142.06 (*C*H), 164.37 (*C*O). HRMS (MALDI-TOF): (M + H)$^+$ calcd for $[C_{27}H_{30}N_4O]H^+$, 427.2498; found, 427.2492. Anal. calcd. for $C_{27}H_{30}N_4O$: C, 76.03; H, 7.09; N, 13.13. Found: C, 75.99; H, 7.23; N, 13.18.

*4.1.4.2. N-(2-aminophenyl)-4-[(4-benzylpiperazin-1-yl)methyl]benzamide (**9a**).* Beige solid (75%): mp 148–150 °C; ^{1}H NMR (500 MHz, $CDCl_3$): δ 2.49 (s, 8H, *H*-piperazine), 3.53 (s, 2H, NC*H*$_2$), 3.57 (s, 2H, NC*H*$_2$), 4.75 (br s, 2H, N*H*$_2$), 6.82–7.32 (m, 9H, Ar*H*), 7.42 (d, J = 15.0 Hz, 2H, Ar*H*), 7.38 (d, J = 15.0 Hz, 2H, Ar*H*), 7.92 (br s, 1H, CON*H*);^{13}C NMR (125 MHz, $CDCl_3$): 52.96 (2*C*H$_2$-piperazine), 53.03 (2*C*H$_2$-piperazine), 62.47 (*C*H$_2$), 62.95 (*C*H$_2$), 118.36 (*C*HAr), 119.75 (*C*HAr), 124.62 (*C*HAr), 125.16 (*C*HAr), 127.08 (*C*HAr), 127.16 (*C*HAr), 127.25 (2*C*HAr), 128.20 (2*C*HAr), 129.23 (2*C*HAr), 129.34 (2*C*HAr), 132.93 (*C-ipso*), 137.83 (*C-ipso*), 140.67 (*C-ipso*), 142.67 (*C*NH$_2$), 165.66 (*C*O). HRMS (MALDI-TOF): (M + H)$^+$ calcd for $[C_{25}H_{28}N_4O]H^+$, 401.2341; found, 401.2348. Anal. calcd. for $C_{25}H_{28}N_4O$: C, 74.97; H, 7.05; N, 13.99. Found: C, 74.77; H, 6.90; N, 14.10.

*4.1.4.3. N-(2-aminophenyl)-4-{[(1-benzylpiperidin-4yl)(methyl)amino] methyl}benzamide(**9b**).* Yellow solid (62%): mp 141–143 °C; ^{1}H NMR (500 MHz, $CDCl_3$): δ 1.60–1.71 (m, 2H, *H*-piperidine), 1.73–1.80 (m, 2H, *H*-piperidine),1.92–2.00 (m, 2H, *H*-piperidine), 2.21 (s, 3H, NC*H*$_3$), 2.38–2.48 (m, 1H, *H*-piperidine), 2.92–3.00 (m, 2H, *H*-piperidine), 3.49 (s, 2H, NC*H*$_2$), 3.63 (m, 2H, NC*H*$_2$), 6.80–7.35 (m, 9H, Ar*H*), 7.42 (d, J = 7.5 Hz,1H, Ar*H*), 7.83 (d, J = 7.5 Hz, 1H, Ar*H*), 7.88 (br s, 1H, CON*H*); ^{13}C NMR (125 MHz, $CDCl_3$): 27.85 (*C*H$_3$), 37.84 (*C*H$_2$-piperidine), 53.22 (2*C*H$_2$-piperidine), 57.62 (2*C*H$_2$-piperidine), 60.95 (*C*H$_2$), 63.04 (*C*H$_2$), 118.30 (*C*HAr), 119.68 (*C*HAr), 124.60 (*C*HAr), 125.21 (*C*HAr), 126.94 (*C*HAr), 127.12 (*C*HAr), 127.25 (2*C*HAr), 128.14 (2*C*HAr), 128.86 (2*C*HAr), 129.13 (2*C*HAr), 132.64 (*C-ipso*), 138.35 (*C-ipso*), 140.72 (*C-ipso*), 144.79 (*C*NH$_2$), 165.77 (*C*O). HRMS (MALDI-TOF): (M + H)$^+$ calcd for $[C_{27}H_{32}N_4O]H^+$, 429.2654.; found, 429.2658. Anal. calcd. for $C_{27}H_{32}N_4O$: C, 75.67; H, 7.53; N, 13.07. Found: C, 75.54; H, 7.47; N, 13.19.

*4.1.5. General procedure for the synthesis of the hydroxyamide (**6, 11a,b**)*

To a solution of esters, **3**, **8a**, or **8b** (1 mmol) in MeOH was added an aqueous solution of LiOH 1 M (2 mmol) dropwise at 50 °C, and the reaction mixture was stirred overnight. The solvent was evaporated under vacuum, and to the resulting residue dissolved in 15 mL of an anhydrous solution of THF/DMF (1:1) was added TEA (2 mmol), followed by the dropwise addition of an ethyl chloroformate solution (4 mmol) in 12 mL of THF at 0 °C and in an inert atmosphere. The reaction was stirred at room temperature for 3 h. Subsequently, *O*-(tetrahydro-2*H*-pyran-2-yl)-hydroxylamine (5 mmol) was added at room temperature under a nitrogen atmosphere, and the reaction was stirred at room temperature overnight. The resulting residue was washed with a saturated solution of $NaHCO_3$, and the aqueous phase was extracted with $CHCl_3$; the combined organic phases were dried with anhydrous Na_2SO_4, filtered, and evaporated under vacuum. The crude was purified by MPLC to obtain the **5**, **10a**, and **10b** intermediates. To a solution of the intermediates in EtOH was added dropwise a solution of HCl 1.25 M in EtOH at 0 °C. The reaction was stirred at room temperature for 24 h. Subsequently, the solvent was evaporated under vacuum, the resulting residue dissolved in EtOH and precipitated with Et_2O. According to this procedure, the following products have been obtained.

4.1.5.1. (E)-3-{4-[(4-benzylpiperazin-1-yl)methyl]phenyl}-N-hydroxyacrylamide hydrochloride (6) [58]. White solid (63%): mp 230–231 °C; ^{1}H NMR (500 MHz, DMSO-d_6): δ 3.21–3.70 (m, 8H, *H*-piperazine), 4.34 (s, 4H, NCH_2), 6.55 (d, J = 16.0 Hz, 1H, COC*H*), 7.44–7.65 (m, 9H + 1H, Ar*H* + ArC*H* = CH), 10.89 (br s, 1H, O*H*), 12.12 (br s, 1H, CON*H*); ^{13}C NMR (125 MHz, DMSO-d_6): δ 47.51 (2CH_2-piperazine), 58.30 (2CH_2-piperazine), 58.72 (CH_2), 79.30 (CH_2), 120.44 (*C*H), 128.12 (*C*HAr), 129.17 (2*C*HAr), 129.32 (2*C*HAr), 130.00 (2*C*HAr), 130.65 (2*C*HAr), 131.58 (*C-ipso*), 132.12 (*C-ipso*), 136.23 (*C-ipso*), 137.89 (*C*H), 162.84 (*C*O). HRMS (MALDI-TOF): (M + H)$^+$ calcd for $[C_{21}H_{25}N_3O_2]H^+$, 352.2025; found, 352.2029. Anal. calcd. for $C_{21}H_{25}N_3O_2{\cdot}2HCl$: C, 59.44; H, 6.41; N, 9.90. Found: C, 59.28; H, 6.50; N, 9.77.

*4.1.5.2. 4-[(4-benzylpiperazin-1-yl)methyl]-N-hydroxybenzamide hydrochloride (**11a**).* White solid (88%): mp 230–232 °C; ^{1}H NMR (500 MHz, DMSO-d_6): δ 3.44 (s, 8H, *H*-piperazine), 4.34 (s, 2H, NCH_2), 4.39 (s, 2H, NCH_2), 7.40–7.54 (m, 5H, Ar*H*), 7.61 (d, J = 5.0 Hz, 2H, Ar*H*), 7.77 (d, J = 8.5 Hz, 2H, Ar*H*), 11.34 (br s, 1H, O*H*) 11.34 (br s, 1H, CON*H*); ^{13}C NMR (125 MHz, $CDCl_3$): δ 47.76 (2CH_2-piperazine), 58.48 (2CH_2-piperazine), 58.97 (CH_2), 79.02 (CH_2), 127.8 (*C*HAr), 129.1 (2*C*HAr), 129.4 (2*C*HAr), 130.3 (2*C*HAr), 131.82 (2*C*HAr), 131.86 (*C-ipso*), 132.73 (*C-ipso*), 133.93 (*C-ipso*), 164.2 (CO). HRMS (MALDI-TOF): (M + H)$^+$ calcd for $[C_{19}H_{23}N_3O_2]H^+$, 326.1868; found, 326.1863. Anal. calcd. for $C_{19}H_{23}N_3O_2{\cdot}2HCl$: C, 57.29; H, 6.33; N, 10.55. Found: C, 57.04; H, 6.21; N, 10.68.

*4.1.5.3. 4-{[(1-benzylpiperidin-4-yl)(methyl)amino]methyl}-N-hydroxybenzamide hydrochloride (**11b**).* Pink solid (93%): mp 229–231 °C; ^{1}H NMR (500 MHz, D_2O): δ 2.15–2.25 (m, 2H, *H*-piperidine), 2.48–2.55 (m, 2H, *H*-piperidine), 2.83 (s, 3H, NCH_3), 3.20–3.30 (m, 2H, *H*-piperidine), 3.58–3.62 (m, 1H, *H*-piperidine), 3.75–3.80 (m, 2H, *H*-piperidine), 4.42 (s, 2H, NCH_2), 4.55 (s, 2H, NCH_2), 7.55–8.15 (m, 9H, Ar*H*); ^{13}C NMR (125 MHz, D_2O):δ 35.76 (CH_3), 50.24 (CH_2-piperidine), 56.81 (2CH_2-piperidine), 59.36 (2CH_2-piperidine), 60.52 (CH_2), 62.53 (CH_2), 65.96, 127.98 (*C*HAr), 128.17 (2*C*HAr), 129.32 (2*C*HAr), 130.37 (2*C*HAr), 131.16 (2*C*HAr), 131.40 (*C-ipso*), 132.66 (*C-ipso*), 133.82 (*C-ipso*), 167.48 (CO). HRMS (MALDI-TOF): (M + H)$^+$ calcd for $[C_{21}H_{27}N_3O_2]H^+$, 354.2181; found, 354.2186. Anal. calcd. for $C_{21}H_{25}N_3O_2{\cdot}2HCl$: C, 59.15; H, 6.86; N, 9.86. Found: C, 59.26; H, 6.83; N, 10.05.

*4.1.6. General procedure for the synthesis of compounds **13a–c***

To a solution of *o*-phenylenediamine (3 mmol) in anhydrous CH_2Cl_2 was added dropwise a solution of the opportune acyl chloride (1 mmol) in 6 mL of CH_2Cl_2 at 0 °C and inert atmosphere, then the reaction mixture was stirred 24 h at room temperature. Subsequently, a saturated solution of $NaHCO_3$was added and the aqueous phase was extracted with CH_2Cl_2. The combined organic phases were dried with anhydrous Na_2SO_4, filtered, and evaporated under vacuum. The crude was purified by flash chromatography with CH_2Cl_2/EtOAc 50:50 in order to obtain the intermediates **12a–c**. The intermediates were added dropwise, under a nitrogen atmosphere, to a solution of 4-(4-chlorophenyl)-4-hydroxypiperidine and K_2CO_3 in anhydrous DMF, and the reaction mixture was stirred 21 h at 80 °C. The solvent was evaporated under vacuum, and the resulting residue was treated with EtOAc and washed with a saturated solution of $NaHCO_3$. The organic and the aqueous phase were repeatedly separated, and the aqueous phase was extracted with EtOAc. The crude was purified by flash chromatography with EtOAc/MeOH 70:30 as eluent. According to this procedure, the following products have been obtained.

4.1.6.1. N-(2-aminophenyl)-3-[4-(4-chlorophenyl)-4-hydroxypiperidin-1-yl]propanamide (13a). White solid (85%): mp 171–174 °C; ^{1}H NMR (500 MHz, DMSO-d_6): δ 1.60–1.57 (m, 2H, *H*-piperidine), 1.96–1.90 (m, 2H, *H*-piperidine), 2.49–2.41 (m, 4H, *H*-piperidine), 2.80–2.78 (m, 2H, NCH_2), 3.33 (m, 2H, COCH_2), 4.99–4.91 (br s, 2H, NH_2), 7.12–6.51 (m, 4H, Ar*H*), 7.51–7.35 (m, 4H, Ar*H*), 9.37 (s, 1H, CON*H*); ^{13}C NMR (125 MHz, DMSO-d_6):δ 33.64 (CH_2), 37.74 (2CH_2-piperidine), 48.79 (2CH_2-piperidine), 54.46 (*C*-piperidine), 69.42 (CH_2), 115.44 (*C*H-Ar), 115.94 (*C*H-Ar), 123.35 (*C*H-Ar), 125.74 (*C*H-Ar), 126.01 (2*C*H-Ar), 126.85 (2*C*H-Ar), 127.69 (C-ipso), 130.76 (*C*H-Ar), 142.70 (*C*H-Ar), 149.04 (*C*NH$_2$), 170.28 (CO). MS (MALDI-TOF): (M + H)$^+$ calcd for $[C_{20}H_{24}ClN_3O_2]H^+$, 374.1635; found, 374.1638. Anal. calcd. for $C_{20}H_{24}ClN_3O_2$: C, 67.21; H, 6.77; N, 11.76. Found: C, 67.43; H, 6.32; N, 11.52.

*4.1.6.2. N-(2-aminophenyl)-3-[4-(4-chlorophenyl)-4-hydroxypiperidin-1-yl]butanamide (**13b**).* White solid (70%): mp 157–160 °C; ^{1}H NMR (500 MHz, DMSO-d_6): δ 1.55–1.53 (m, 2H, *H*-piperidine), 1.77 (m, 2H, *H*-piperidine), 1.91–1.85 (m, 2H, *H*-piperidine), 2.37–2.33 (m, 6H, CH_2) 2.67–2.65 (m, 2H, *H*-piperidine), 3.51 (br s, 1H, O*H*), 4.85 (br s, 2H, NH_2), 7.20–6.51 (m, 4H, Ar*H*), 7.45–7.32 (m, 4H, Ar*H*), 9.21 (s, 1H, CONH$_2$); ^{13}C NMR (125 MHz, DMSO-d_6): δ 22.67 (CH_2), 34.07 (CH_2), 37.92 (CH_2), 48.99 (2CH_2-piperidine), 57.59 (2CH_2-piperidine), 69.56 (*C*-piperidine), 115.77 (*C*H-Ar), 116.06 (*C*H-Ar), 123.68 (2*C*H-Ar), 125.08 (*C*H-Ar), 125.48 (2*C*H-Ar), 126.78 (2*C*H-Ar), 127.62 (*C*Cl), 130.64 (*C*-ipso), 141.76 (*C*H-Ar), 149.21 (*C*NH$_2$), 171.15 (CO). HRMS (MALDI-TOF): (M + H)$^+$ calcd for $[C_{21}H_{26}ClN_3O_2]H^+$, 388.1792; found, 388.1797. Anal. calcd. for $C_{21}H_{26}N_3O_2$: C, 67.90; H, 7.06; N, 11.31. Found: C, 68.18; H, 6.88; N, 11.15.

*4.1.6.3. N-(2-aminophenyl)-3-[4-(4-chlorophenyl)-4-hydroxypiperidin-1-yl]pentanamide (**13c**).* White solid (60%): mp 163–166 °C; ^{1}H NMR (500 MHz, DMSO-d_6): δ 1.64–1.46 (m, 6H, *H*-piperidine), 1.91–1.85 (m, 2H, *H*-piperidine), 2.36–2.32 (m, 6H, CH_2), 2.65–2.63 (m, 2H, COCH_2), 3.43 (br s, 1H, O*H*), 4.82 (br s, 2H, NH_2), 7.16–6.51 (m, 4H, Ar*H*), 7.49–7.33 (m, 4H, Ar*H*), 9.15 (s, 1H, CON*H*); ^{13}C NMR (125 MHz, DMSO-d_6): δ 23.40 (CH_2), 26.13 (CH_2), 35.63 (CH_2), 37.92 (CH_2), 49.04 (2CH_2-piperidine), 57.83 (2CH_2-piperidine), 69.55 (*C*-piperidine), 115.84 (*C*H-Ar), 116.11 (*C*H-Ar), 123.58 (2*C*H-Ar), 125.19 (*C*H-Ar), 125.60 (2*C*H-Ar), 126.82 (*C*H-Ar), 127.65 (2*C*H-Ar), 130.67 (2*C*H-Ar), 141.84 (*C*Cl), 149.21 (*C*NH$_2$), 171.12 (CO). HRMS (MALDI-TOF): (M + H)$^+$ calcd for $[C_{22}H_{28}ClN_3O_2]H^+$, 402.1948; found, 402.1943. Anal. calcd. for $C_{22}H_{28}N_3O_2$: C, 65.74; H, 7.02; N, 10.45. Found: C, 65.97; H, 6.78; N, 10.28.

4.2. Receptors radioligand binding assays

4.2.1. Materials

Brain and liver homogenates for σ_1R and σ_2R receptor binding assays were prepared from male Dunkin-Hartley guinea pigs and Sprague Dawley rats, respectively (ENVIGO RMS S.R.L., Udine, Italy). Animals (200–250 g) were euthanized with CO_2 in a euthanasia chamber and sacrificed by decapitation. Guinea pig brains without cerebellum (~2.5 g each) and rat livers (~7 g each) were kept on dry ice and stored at –80 °C. [^{3}H](+)-Pentazocine (26.9 Ci/mmol) and [^{3}H]1,3-di-*o*-tolylguanidine ([^{3}H]DTG, 35.5 Ci/mmol) were purchased from PerkinElmer (Zaventem, Belgium). Ultima Gold MV Scintillation cocktail was from PerkinElmer (Milan, Italy). All the other materials were obtained from Merck Life Science S.r.L. (Milan, Italy). The test compound solutions were prepared by dissolving approximately 10 μmol of the test compound in DMSO so that a 10 mM stock solution was obtained. The required test concentrations for the assay (from 10^{-5} to 10^{-11} M) have been prepared by diluting the DMSO stock solution with the respective assay buffer. All experiments were performed using ultrapure water obtained with a Millipore Milli-Q Reference Ultrapure Water Purification System. All the laboratory glassware was first washed with 6 M HCl water solution and then rinsed with ultrapure water.

4.2.2. Preparation of membrane homogenates from pig brain

Fresh guinea pig brain cortices (~25 g) were homogenized in two portions with 10 volumes of ice-cold Tris (50 mM, pH 7.4) containing 0.32 M sucrose with a Potter-Elvehjem glass homogenizer. The suspension was centrifuged at 1,030 × g for 10 min at 4 °C. The supernatant was separated and centrifuged at 41,200 × g for 20 min at 4 °C. The obtained pellet was suspended with 3 volumes of ice-cold Tris (50 mM, pH 7.4), incubated at rt for 15 min, and centrifuged at 41,200 × g for 15 min at 4 °C. The final pellet was resuspended with ~ 2 volumes of ice-cold Tris buffer and frozen at –80 °C in ~ 1 mL portions containing about 5 mg protein/mL.

4.2.3. Preparation of membrane homogenates from rat liver

Rat livers (~21 g) were cut into small pieces with a scalpel and homogenized in two portions with 6 volumes of cold 0.32 M sucrose with a Potter-Elvehjem glass homogenizer. The suspension was centrifuged at 1,030 × g for 10 min at 4 °C. The supernatant was separated and centrifuged at 31,100 × g for 20 min at 4 °C. The pellet was resuspended with 6 volumes of ice-cold Tris buffer (50 mM, pH 8) and incubated at rt for 30 min. Then, the suspension was centrifuged at 31,100 × g for 20 min at 4 °C. The final pellet was resuspended with 6 volumes of ice-cold Tris buffer and stored at –80 °C in ~ 1 mL portions containing about 6 mg protein/mL.

4.2.4. Protein determination

The protein concentration was determined by the Bradford method. The Bradford solution was prepared by dissolving 10 mg of Coomassie Brilliant Blue G 250 in 5 mL of 95% ethanol. To this solution, 10 mL of 85% phosphoric acid were added, and the mixture was stirred and filled to a total volume of 100 mL with ultrapure water. The calibration was carried out with bovine serum albumin, as a standard, at different concentrations. In a 96-well plate, 30 μL of the calibration solution or 30 μL of the membrane receptor preparation were mixed with 240 μL of the Bradford solution, respectively. After 5 min of incubation at rt, the UV absorbance was measured at λ = 595 nm using a microplate spectrophotometer reader (Synergy HT, BioTek).

4.2.5. σ_1R ligand binding assays

In vitro σ_1R ligand binding assays were carried out in Tris buffer (50 mM, pH 7.4) for 150 min at 37 °C. The thawed membrane preparation of the guinea pig brain cortex (250 μg/sample) was incubated with increasing concentrations of test compounds and [^{3}H](+)-pentazocine (2 nM) in a final volume of 0.5 mL. The K_d value of [^{3}H](+)-pentazocine was 2.9 nM. Unlabeled (+)-pentazocine (10 μM) was used to measure non-specific binding. Bound and free radioligand were separated by fast filtration under reduced pressure using a Millipore filter apparatus through Whatman GF/6 glass fiber filters, which were presoaked in a 0.5% poly(ethyleneimine) water solution for 120 min. Each filter paper was rinsed three times with 3 mL ice-cold Tris buffer (50 mM, pH 7.4), dried at rt, and incubated overnight with 3 mL scintillation cocktail into pony vials. The bound radioactivity has been determined using a liquid scintillation counter (Beckman LS 6500).

4.2.6. σ_2R ligand binding assays

In vitro, σ_2R ligand binding assays were carried out in Tris buffer (50 mM, pH 8.0) for 120 min at rt. The thawed membrane preparation of rat liver (250 μg/sample) was incubated with increasing concentrations of test compounds and [^{3}H]DTG (2 nM) in the presence of (+)-pentazocine (5 μM) as σ_1R masking agent in a final volume of 0.5 mL. The K_d value of [^{3}H]DTG was 17.9 nM. Non-specific binding was evaluated with unlabeled DTG (10 μM). Bound and free radioligand were separated by fast filtration under reduced pressure using a Millipore filter apparatus through Whatman GF/6 glass fiber filters, which were presoaked in a 0.5% poly(ethyleneimine) water solution for 120 min. Each filter paper was rinsed three times with 3 mL ice-cold Tris buffer (10 mM, pH 8), dried at rt, and incubated overnight with 3 mL scintillation cocktail into pony vials. The bound radioactivity has been determined using a liquid scintillation counter (Beckman LS 6500).

4.2.7. Data analysis

The K_i-values were calculated using GraphPad Prism® 7.0 (GraphPad Software, San Diego, CA, USA). The K_i-values are given as mean value ± SD from at least two independent experiments performed in duplicate.

4.3. In vitro pharmacology

4.3.1. Cell culture and seeding

AGS (human gastric adenocarcinoma) and PC3 (human prostate adenocarcinoma) cell lines were purchased from ECACC and maintained in HAM's F12medium supplemented with 10% of fetal bovine serum (FBS) and 1% of penicillin/streptomycin (Gibco - Thermofisher Scientific, MD, USA).Human breast cancer MCF7 (HTB-22™), human colorectal carcinoma cell line HCT116, and human keratinocytes cell line HaCaT were purchased by ATCC and maintained in Dulbecco's modified Eagle's medium (DMEM) high glucose (EuroClone, Milan, Italy) supplemented with10% of fetal bovine serum (FBS) and 1% of penicillin/streptomycin (Gibco - Thermofisher Scientific).All the cells were maintained in a humified atmosphere of 5% CO_2 at 37 °C.After reaching the exponential growth phase, the cells were seeded into 96/wellculture plates at different densities: AGS and MCF7 at 10000/well, HaCaT 8000/well, PC3 6000/well, and HCT116 5000/mL, according to their different growth rate and previous experience. The cells were left to adhere for 24 h, and then the medium was replaced with the same volume of medium with the indicated concentration of compounds, as described in the following paragraph.

4.3.2. Cell treatment and MTT assay

First, AGS cells were treated with different concentrations, ranging 0.1–10 μM, of all the previously described compounds. An MTT assay was performed at 24, 48, and 72 h.Second, all the four cancer cell lines (AGS, HCT116, MCF7, and PC3) were exposed to different concentrations (range 0–80 μM) of compounds **6**, **9a**, and **9b**. An MTT assay was performed at 48 h, and the IC_{50} for each compound for each cell line was calculated using GraphPad Prism software.Third, all the four cancer cell lines (AGS, HCT116, MCF7, and PC3) were exposed to different concentrations (0–80 μM) of **6**, **9a**, **9b**, VPA, and BD1063, both alone and in an equimolar solution and an MTT assay was performed at 48 h.Last, HaCaT cells were exposed to different concentrations (0–80 μM) of

compounds **6** and **9b**,and an MTT assay was performed at 48 h. Cell viability was assessed by MTT (3-(4,5-dimethylthiazol-2-yl)-2,5-diphenyltetrazoliumbromide) test (Sigma Aldrich, Milan, Italy). At the indicated experimental times, cells were incubated with 100 mL/well of MTT (1 mg/mL) 1:10 with a fresh growth medium for 4 h at 37 °C and 5% CO_2. Finally, the MTT solution was removed and replaced with 100 mL/well of DMSO. Cells were incubated for an additional 20 min at 37 °C and 5% CO_2 and gently swirled for 10 min at room temperature. The optical density was measured at 540 nm employing a spectrophotometer (Multiskan GO, Thermo Scientific, Monza, Italy). The results were expressed as the percentage of control cells, and each experiment was performed three times in triplicate.

4.3.3. Statistical analysis

All results are reported as mean ± SD from at least three independent experiments (n = 3) performed at least in triplicate. The results were analyzed using oneway ANOVA followed by Tukey–Kramer multiple comparisons test; differences between groups were considered significant for p-value < 0.05.

4.3.4. HDAC activity assay

AGS, HCT116, MCF7, and PC3cells were harvested and centrifuged. Pellets were rinsed twice in PBS and lysed in 400 μL sterile water 10 min. HDAC activity was investigated in cell lysates from 50 μg total protein using BioVision HDAC Activity Colorimetric Assay kit (Catalog #K331-100), according to the manufacturer's protocol. Cell lysates were prepared from all cancer cell lines, and all procedures were performed at 4 °C. Briefly, cells (AGS 18 × 10^6, PC3 32 × 10^6, MCF7 10 × 10^6, HCT116 67 × 10^6) were washed twice with ice-cold PBS and resuspended as 5 × 10^7cells/mL of lysis buffer (120 mM NaCl, 50 m M Tris (pH 7.5), 5 mM EDTA, and 0.5% (v/v) Nonidet P-40) in the presence of freshly added protease inhibitors (2 μg/mL aprotinin, 1 μg/mL leupeptin, 1 mM Sodium orthovanadate and 0.5 mM PMSF). After 30 min, the suspension was passed 10 times through a 21 gauge needle, and PMSF was added (1:200).The lysates were incubated for 30 min in ice and then cleared by centrifugation at 10,000 × g for 10 min at 4 °C. The supernatants were stored at –80 °C. Protein concentration was determined with QuantiProTM BCA Assay Kit (Cat. No. QPBCA). Using 96-well plates with a U-shape bottom, 150 μg of cell lysate was diluted to 85 μL (final volume) of ddH_2O in each well (for background reading, add 85 μL ddH_2O only). Each cell lysate was diluted to 83 μL, and 2 μL of each compound (1 mM) was added. 10 μL of the 10X HDAC Assay Buffer was added, followed by 5 μL of the HDAC colorimetric substrate to each well and mixed thoroughly. The plate was incubated at 37 °C for 3.5 h. The reaction was stopped by adding 10 μL of Lysine Developer, and the plate was incubated at 37 °C for a further 30 min. The samples were read in an ELISA plate reader at 405 nm (Multiskan GO), and HDAC activity was expressed as the relative O.D. value.The IC_{50} values were calculated using GraphPad Prism® software at different concentrations (0–20 μM).

4.4. Evaluation of chemical stability

4.4.1. Chromatographic conditions

The chromatographic analyses were performed using Agilent 1260 Infinity II HPLC (Agilent, Santa Clara, CA, USA) consisting of a 1260 Infinity II Quaternary Pump (model G7111A), 1260 Infinity II autosampler (model G7129A), 1260 Infinity II Multicolumn Thermostat (model G7116A), and 1260 Infinity II Diode Array Detector (model G7115A). Results were collected and integrated using an Agilent OpenLAB CDS LC ChemStation software. Poroshell 120 EC-C18 column (150 × 4.6 mm i.d., particle size 4 μm; Agilent, Santa Clara, USA) was used for the separations. Samples were analyzed using a mixture of water/acetonitrile, enriched with trifluoroacetic acid (0.1% v/v) as mobile phase, in a gradient elution mode starting from 80% to 20% of water over 12 min. The flow rate was 0.8 mL/min. The UV detector was set at a length of 254 nm. The stock solutions used to define the purity of each compound were prepared by dissolving the selected entities in an acidified aqueous medium.

4.4.2. Kinetic of chemical hydrolysis

Phosphate (PBS, pH 7.4) and hydrochloric acid buffers (pH 1.3) were used to evaluate the chemical stability at physiological pH. The reaction was initiated by adding 1 mL of 2 × 10^{-4} M stock solution of the compound to 10 mL of thermostated (37 ± 0.5 °C) aqueous buffer solution. At established time points, samples (20 μL) were withdrawn and analyzed by HPLC. Pseudo-first-order rate constants (k_{obs}) for the hydrolysis of the compounds were calculated from the slopes of the linear plots of log (% residual compound) against time. The analyses were held in triplicate, and the rate constants' mean values were calculated.

4.4.3. Kinetics of enzymatic hydrolysis

Human plasma was obtained from 3H Biomedical (Uppsala, Sweden, Europe). Each compound (125 μg/mL) was added to plasma fractions (1.6 mL) diluted with 400 μL of PBS (pH 7.4) to obtain a final volume of 2 mL (80% of plasma). Studies were performed at 37 ± 0.5 °C using a shaking bath. Aliquots (100 μL) were taken at established time points and treated with cold methanol (200 μL). After centrifugation for 15 min at 5000 g, the supernatant was analyzed by HPLC. The amounts of the remaining intact compound were plotted as a function of incubation time.

4.4.4. ADME profile

SwissADME (www.swissadme.ch accessed on 7 October 2021) was used to predict the ADME profile of the selected compounds [59]. SMILES notations were generated with MarvinSketch (18.24, ChemAxon Ltd., Budapest, Hungary)software. Consequently, submitted as input to the Swiss ADME online program, molecular parameters such as solubility, LogP, permeation through the blood-brainbarrier (BBB) and gastrointestinal (GI) tract, skin permeability, CYP inhibition, and accordance to Lipinski filter were evaluated.

4.5. Computational studies

4.5.1. Ligands preparation

The structures of compounds **6** and **9b** were built using MarvinSketch (18.24, ChemAxon Ltd., Budapest, Hungary). All the protonation states were calculated, assuming a physiological pH of 7.4 (Table S3), and then prepared using Autodock Tools 1.5.6.[60] The PM6-D3H4 Hamiltonian, as implemented in the MOPAC package (MOPAC2016 v. 18.151, Stewart Computational Chemistry, Colorado Springs, CO, USA), [61] was then used to further optimize the 3D structures before the alignment for the docking calculations. Partial Gasteiger atomic charges were assigned to the compounds.[62] Trichostatin A (TSA), the most important pan-HDACi, was included as a positive control in the modeling studies, and its structure was also prepared as previously described for the other compounds.

4.5.2. Selections of HDAC models

The 3D coordinates of human HDACs available at the time of the present study were downloaded from the Protein Data Bank (PDB) platform at the address https://www.rcsb.org/ (accessed on 30 June 2021): HDAC1 (PDB ID: 4BKX) [63], HDAC2 (PDB ID: 7KBG) [64], HDAC3 (PDB ID: 4A69) [65], HDAC4 (PDB ID: 6FYZ) [66], HDAC6 (PDB ID: 5EDU) [67], HDAC7 (PDB ID: 3C0Y) [68], HDAC8 (PDB ID: 5FCW) [69]. For the X-ray targets selection, the following criteria were respected: (1) the origin from Homo Sapiens; (2) minimum missing regions; (3) the absence of mutations and covalent co-crystallized ligands; (4) the best Diffraction-component Precision Index (DPI) score (Table S2) [70]. Thus, we considered only the 3D structures experimentally reported in the PDB. At the same time, the catalytic domain of HDAC5 and HDAC9 for class IIa, and HDAC10 for class IIb, were not included due to the lack of crystallographic information. Then, each

crystallographic model was prepared using AutoDock Tools 1.5.6 [60], by encompassing polar hydrogen atoms and Kollman [71] charges in the HDACs structure.

4.5.3. Molecular docking

Flexible ligands docking experiments were performed employing AutoDock Vina implemented in YASARA, using the crystal structure of the human σ_1 receptor model bound to PD144418 (PDB 5HK1) retrieved from the PDB_REDO Data Bank. Docking for the σ_2 receptor was performed using the homology models previously built by the same authors [72].

Molecular modeling calculations were performed using Autodock 4.2.6 software [60] and Autodock4 Zn force-field, which contains improved parameters for the docking of zinc metalloenzymes [73]. In particular, for each HDAC model, the grid box of 60 $Å^3$ was centered on the zinc cation within the catalytic cavity. Then, the maps were generated by AutoGrid (4.2.6) with a spacing of 0.375 Å and dimensions encompassing all the active site's surface. All the parameters were inserted at their default settings. Thus, the most populated cluster with the lowest free energy of binding values was chosen and analyzed. The docking protocol was validated by applying the re-docking procedure to the PDB models containing a co-crystallized ligand (HDAC2, HDAC4, HDAC6, HDAC7, and HDAC8) and by evaluating the Root Mean Square Deviation (RMSD) between the X-ray and the docking pose of each ligand (Table S4).

Funding

This work was financially supported by Italian MUR, PON FSE–FESR R&I funds 2014–2020 Action I. 1 (CUP: E77H18000450006, DOT1708221, grant 3) and PRIN 2017, Code 201744BN5T.

Declaration of Competing Interest

The authors declare that they have no known competing financial interests or personal relationships that could have appeared to influence the work reported in this paper.

Data availability

No data was used for the research described in the article.

Appendix A. Supplementary data

Supplementary data to this article can be found online at https://doi.org/10.1016/j.bioorg.2023.106794.

References

[1] J. Olsen, K. Overvad, The concept of multifactorial etiology of cancer, Pharmacol. Toxicol. 72 (Suppl 1) (1993) 33–38.
[2] A. Cavalli, M.L. Bolognesi, A. Minarini, M. Rosini, V. Tumiatti, M. Recanatini, C. Melchiorre, Multi-target-directed ligands to combat neurodegenerative diseases, J. Med. Chem. 51 (3) (2008) 347–372.
[3] J.-U. Peters, Polypharmacology - foe or friend? J. Med. Chem. 56 (22) (2013) 8955–8971.
[4] H. Daub, K. Specht, A. Ullrich, Strategies to overcome resistance to targeted protein kinase inhibitors, Nat. Rev. Drug Discov. 3 (12) (2004) 1001–1010.
[5] A. Kamb, S. Wee, C. Lengauer, Why is cancer drug discovery so difficult? Nat. Rev. Drug Discov. 6 (2) (2007) 115–120.
[6] W. Zhang, J. Pei, L. Lai, Computational Multitarget Drug Design, J. Chem. Inf. Model. 57 (2017) 403–412.
[7] W.D. Bowen, Sigma receptors: recent advances and new clinical potentials, Pharm. Acta Helv. 74 (2-3) (2000) 211–218.
[8] H.M. Oyer, C.M. Sanders, F.J. Kim, Small-Molecule Modulators of Sigma1 and Sigma2/TMEM97 in the Context of Cancer: Foundational Concepts and Emerging Themes, Front. Pharmacol. 10 (2019) 1141.
[9] A.N. Fallica, V. Pittala, M.N. Modica, L. Salerno, G. Romeo, A. Marrazzo, M. A. Helal, S. Intagliata, Recent Advances in the Development of Sigma Receptor Ligands as Cytotoxic Agents: A Medicinal Chemistry Perspective, J. Med. Chem. 64 (2021) 7926–7962.
[10] D. Crottes, H. Guizouarn, P. Martin, F. Borgese, O. Soriani, The sigma-1 receptor: a regulator of cancer cell electrical plasticity? Front. Physiol. 4 (2013) 175.
[11] H.R. Schmidt, S. Zheng, E. Gurpinar, A. Koehl, A. Manglik, A.C. Kruse, Crystal structure of the human sigma1 receptor, Nature 532 (2016) 527–530.
[12] T. Hayashi, T.P. Su, Sigma-1 receptor chaperones at the ER-mitochondrion interface regulate Ca(2+) signaling and cell survival, Cell 131 (2007) 596–610.
[13] T.P. Su, T. Hayashi, T. Maurice, S. Buch, A.E. Ruoho, The sigma-1 receptor chaperone as an inter-organelle signaling modulator, Trends Pharmacol. Sci. 31 (2010) 557–566.
[14] T. Maurice, T.P. Su, The pharmacology of sigma-1 receptors, Pharmacol. Ther. 124 (2009) 195–206.
[15] T. Maurice, Improving Alzheimer's disease-related cognitive deficits with sigma 1 receptor agonists, Drug News Perspect. 15 (2002) 617–625.
[16] P. Orazio, A. Emanuela, S.-F. Cristine, T. Rita, P. Carmela, M. Agostino, C. Roberto, A. Emanuele, P. Lorella, (+)-and (−)-Phenazocine enantiomers: evaluation of their dual opioid agonist/σ1 antagonist properties and antinociceptive effects, Eur. J. Med. Chem. 125 (2017).
[17] U.B. Chu, A.E. Ruoho, Biochemical Pharmacology of the Sigma-1 Receptor, Mol. Pharmacol. 89 (2016) 142–153.
[18] M. Olivieri, E. Amata, S. Vinciguerra, J. Fiorito, G. Giurdanella, F. Drago, N. Caporarello, O. Prezzavento, E. Arena, L. Salerno, A. Rescifina, G. Lupo, C. D. Anfuso, A. Marrazzo, Antiangiogenic Effect of (+/-)-Haloperidol Metabolite II Valproate Ester [(+/-)-MRJF22] in Human Microvascular Retinal Endothelial Cells, J. Med. Chem. 59 (2016) 9960–9966.
[19] A. Marrazzo, J. Fiorito, L. Zappala, O. Prezzavento, S. Ronsisvalle, L. Pasquinucci, G.M. Scoto, R. Bernardini, G. Ronsisvalle, Antiproliferative activity of phenylbutyrate ester of haloperidol metabolite II [(+/-)-MRJF4] in prostate cancer cells, Eur. J. Med. Chem. 46 (2011) 433–438.
[20] A. Alon, H.R. Schmidt, M.D. Wood, J.J. Sahn, S.F. Martin, A.C. Kruse, Identification of the gene that codes for the sigma2 receptor, PNAS 114 (2017) 7160–7165.
[21] A. Alon, J. Lyu, J.M. Braz, T.A. Tummino, V. Craik, M.J. O'Meara, C.M. Webb, D. S. Radchenko, Y.S. Moroz, X.-P. Huang, Y. Liu, B.L. Roth, J.J. Irwin, A.I. Basbaum, B.K. Shoichet, A.C. Kruse, Structures of the σ2 receptor enable docking for bioactive ligand discovery, Nature 600 (2021) 759–764.
[22] A. Van Waarde, A.A. Rybczynska, N. Ramakrishnan, K. Ishiwata, P.H. Elsinga, R. A. Dierckx, Sigma receptors in oncology: therapeutic and diagnostic applications of sigma ligands, Curr. Pharm. Des. 16 (2010) 3519–3537.
[23] R.H. Mach, C. Zeng, W.G. Hawkins, The sigma2 receptor: a novel protein for the imaging and treatment of cancer, J. Med. Chem. 56 (2013) 7137–7160.
[24] B.J. Vilner, C.S. John, W.D. Bowen, Sigma-1 and Sigma-2 Receptors Are Expressed in a Wide Variety of Human and Rodent Tumor-Cell Lines, Cancer Res. 55 (1995) 408–413.
[25] T.C.S. Ho, A.H.Y. Chan, A. Ganesan, Thirty Years of HDAC Inhibitors: 2020 Insight and Hindsight, J. Med. Chem. 63 (2020) (2020) 12460–12484.
[26] K.J. Falkenberg, R.W. Johnstone, Histone deacetylases and their inhibitors in cancer, neurological diseases and immune disorders, Nat. Rev. Drug Discov. 13 (2014) 673–691.
[27] T. Kouzarides, Chromatin modifications and their function, Cell 128 (2007) 693–705.
[28] S. Zhao, W. Xu, W. Jiang, W. Yu, Y. Lin, T. Zhang, J. Yao, L. Zhou, Y. Zeng, H. Li, Y. Li, J. Shi, W. An, S.M. Hancock, F. He, L. Qin, J. Chin, P. Yang, X. Chen, Q. Lei, Y. Xiong, K.L. Guan, Regulation of cellular metabolism by protein lysine acetylation, Science 327 (2010) 1000–1004.
[29] A.S. Truong, M. Zhou, B. Krishnan, T. Utsumi, U. Manocha, K.G. Stewart, W. Beck, T.L. Rose, M.I. Milowsky, X. He, C.C. Smith, L.M. Bixby, C.M. Perou, S.E. Wobker, S.T. Bailey, B.G. Vincent, W.Y. Kim, Entinostat induces antitumor immune responses through immune editing of tumor neoantigens, J. Clin. Invest. 131 (2021).
[30] J.P. Laubach, P. Moreau, J.F. San-Miguel, P.G. Richardson, Panobinostat for the Treatment of Multiple Myeloma, Clin. Cancer Res. 21 (2015) 4767–4773.
[31] B.S. Mann, J.R. Johnson, M.H. Cohen, R. Justice, R. Pazdur, FDA approval summary: vorinostat for treatment of advanced primary cutaneous T-cell lymphoma, Oncologist 12 (2007) 1247–1252.
[32] K.M. VanderMolen, W. McCulloch, C.J. Pearce, N.H. Oberlies, Romidepsin (Istodax, NSC 630176, FR901228, FK228, depsipeptide): a natural product recently approved for cutaneous T-cell lymphoma, J. Antibiot. (Tokyo) 64 (2011) 525–531.
[33] C. Barbaraci, G. Giurdanella, C.G. Leotta, A. Longo, E. Amata, M. Dichiara, L. Pasquinucci, R. Turnaturi, O. Prezzavento, I. Cacciatore, E. Zuccarello, G. Lupo, G.M. Pitari, C.D. Anfuso, A. Marrazzo, Haloperidol Metabolite II Valproate Ester (S)-(-)-MRJF22: Preliminary Studies as a Potential Multifunctional Agent Against Uveal Melanoma, J. Med. Chem. 64 (2021) 13622–13632.
[34] G.F. Mangiatordi, F. Intranuovo, P. Delre, F.S. Abatematteo, C. Abate, M. Niso, T. M. Creanza, N. Ancona, A. Stefanachi, M. Contino, Cannabinoid Receptor Subtype 2 (CB2R) in a Multitarget Approach: Perspective of an Innovative Strategy in Cancer and Neurodegeneration, J. Med. Chem. 63 (2020) 14448–14469.
[35] D.A. Rodrigues, P.S.M. Pinheiro, C.A.M. Fraga, Multitarget Inhibition of Histone Deacetylase (HDAC) and Phosphatidylinositol-3-kinase (PI3K): Current and Future Prospects, ChemMedChem 16 (2021) 448–457.
[36] V. Ivasiv, C. Albertini, A.E. Gonçalves, M. Rossi, M.L. Bolognesi, Molecular Hybridization as a Tool for Designing Multitarget Drug Candidates for Complex Diseases, Curr. Top. Med. Chem. 19 (2019) 1694–1711.
[37] R.A. Glennon, Pharmacophore identification for sigma-1 (sigma1) receptor binding: application of the "deconstruction-reconstruction-elaboration" approach, Mini Rev. Med. Chem. 5 (2005) 927–940.
[38] B. Wunsch, Pharmacophore models and development of spirocyclic ligands for σ1 receptors, Curr. Pharm. Des. 18 (2012) 930–937.

[39] T.A. Miller, D.J. Witter, S. Belvedere, Histone deacetylase inhibitors, J. Med. Chem. 46 (2003) 5097–5116.
[40] A. Mai, S. Massa, D. Rotili, R. Pezzi, P. Bottoni, R. Scatena, J. Meraner, G. Brosch, Exploring the connection unit in the HDAC inhibitor pharmacophore model: novel uracil-based hydroxamates, Bioorg. Med. Chem. Lett. 15 (21) (2005) 4656–4661.
[41] Z. Peng, Q. Zhao, X. Tian, T. Lei, R. Xiang, L. Chen, Y. Yang, Discovery of Potent and Isoform-selective Histone Deacetylase Inhibitors Using Structure-based Virtual Screening and Biological Evaluation, Mol Inform 41 (9) (2022) e2100295.
[42] G. Gopal, U.M. Raja, S. Shirley, K.R. Rajalekshmi, T. Rajkumar, SOSTDC1 down-regulation of expression involves CpG methylation and is a potential prognostic marker in gastric cancer, Cancer Genet. 206 (2013) 174–182.
[43] M. Yarim, M. Koksal, D. Schepmann, B. Wunsch, Synthesis and in vitro Evaluation of Novel Indole-Based Sigma Receptors Ligands, Chem. Biol. Drug Des. 78 (2011) 869–875.
[44] D. Qu, M. Jiao, H. Lin, C. Tian, G. Qu, J. Xue, L. Xue, C. Ju, C. Zhang, Anisamide-functionalized pH-responsive amphiphilic chitosan-based paclitaxel micelles for sigma-1 receptor targeted prostate cancer treatment, Carbohydr. Polym. 229 (2020), 115498.
[45] F.E. Oflaz, Z. Koshenov, M. Hirtl, R. Rost, R. Malli, W.F. Graier, Sigma-1 Receptor Modulation by Ligands Coordinates Cancer Cell Energy Metabolism, Biomolecules 12 (6) (2022) 762.
[46] F. Giordano, A. Paoli, M. Forastiero, S. Marsico, F. De Amicis, M. Marrelli, G. D. Naimo, L. Mauro, M.L. Panno, Valproic acid inhibits cell growth in both MCF-7 and MDA-MB231 cells by triggering different responses in a cell type-specific manner, J. Transl. Med. 21 (2023) 165.
[47] R. Mahalakshmi, P. Husayn Ahmed, V. Mahadevan, HDAC inhibitors show differential epigenetic regulation and cell survival strategies on p53 mutant colon cancer cells, J. Biomol. Struct. Dyn. 36 (4) (2018) 938–955.
[48] M. Rui, D. Rossi, A. Marra, M. Paolillo, S. Schinelli, D. Curti, A. Tesei, M. Cortesi, A. Zamagni, E. Laurini, S. Pricl, D. Schepmann, B. Wunsch, E. Urban, V. Pace, S. Collina, Synthesis and biological evaluation of new aryl-alkyl(alkenyl)-4-benzylpiperidines, novel Sigma Receptor (SR) modulators, as potential anticancer-agents, Eur. J. Med. Chem. 124 (2016) 649–665.
[49] I. Cacciatore, L. Baldassarre, E. Fornasari, C. Cornacchia, A. Di Stefano, P. Sozio, L. S. Cerasa, A. Fontana, S. Fulle, E.S. Di Filippo, R.M. La Rovere, F. Pinnen, (R)-alpha-lipoyl-glycyl-L-prolyl-L-glutamyl dimethyl ester codrug as a multifunctional agent with potential neuroprotective activities, ChemMedChem 7 (2012) 2021–2029.
[50] S. Ramachandran, U.B. Chu, T.A. Mavlyutov, A. Pal, S. Pyne, A.E. Ruoho, The sigma1 receptor interacts with N-alkyl amines and endogenous sphingolipids, Eur. J. Pharmacol. 609 (1-3) (2009) 19–26.
[51] A. Maruca, F.A. Ambrosio, A. Lupia, I. Romeo, R. Rocca, F. Moraca, C. Talarico, D. Bagetta, R. Catalano, G. Costa, A. Artese, S. Alcaro, Computer-based techniques for lead identification and optimization I: Basics, Physical Sciences Reviews 4 (2019).
[52] G. Costanzo, V. Patamia, R. Turnaturi, C. Parenti, C. Zagni, J. Lombino, E. Amata, A. Marrazzo, L. Pasquinucci, A. Rescifina, Design, synthesis, in vitro evaluation, and molecular modeling studies of N-substituted benzomorphans, analogs of LP2, as novel MOR ligands, Chem. Biol. Drug Des. (2023).
[53] V. Patamia, G. Floresta, C. Zagni, V. Pistara, F. Punzo, A. Rescifina, 1,2-Dibenzoylhydrazine as a Multi-Inhibitor Compound: A Morphological and Docking Study, Int. J. Mol. Sci. 24 (2023).
[54] K. Szczepanska, S. Podlewska, M. Dichiara, D. Gentile, V. Patamia, N. Rosier, D. Monnich, M.C. Ruiz Cantero, T. Karcz, D. Lazewska, A. Siwek, S. Pockes, E. J. Cobos, A. Marrazzo, H. Stark, A. Rescifina, A.J. Bojarski, E. Amata, K. Kiec-Kononowicz, Structural and Molecular Insight into Piperazine and Piperidine Derivatives as Histamine H(3) and Sigma-1 Receptor Antagonists with Promising Antinociceptive Properties, ACS Chem. Nerosci. 13 (2022) 1–15.
[55] A. Maruca, F. Moraca, R. Rocca, F. Molisani, F. Alcaro, M.C. Gidaro, S. Alcaro, G. Costa, F. Ortuso, Chemoinformatic Database Building and in Silico Hit-Identification of Potential Multi-Targeting Bioactive Compounds Extracted from Mushroom Species, Molecules 22 (2017) 1571.
[56] C. Zhao, H. Dong, Q. Xu, Y. Zhang, Histone deacetylase (HDAC) inhibitors in cancer: a patent review (2017-present), Expert Opin. Ther. Pat. 30 (2020) 263–274.
[57] X. Li, Y.K. Peterson, E.S. Inks, R.A. Himes, J. Li, Y. Zhang, X. Kong, C.J. Chou, Class I HDAC Inhibitors Display Different Antitumor Mechanism in Leukemia and Prostatic Cancer Cells Depending on Their p53 Status, J. Med. Chem. 61 (2018) 2589–2603.
[58] SC Cho, L Jiang, M Shultz, CHT Chen, G Liu, J Li, inventors, J Dyer, AG Novartis, assignee. Hydroxamate-based inhibitors of deacetylases. US patent 12/870,123 3 (2012 March).
[59] A. Daina, O. Michielin, V. Zoete, SwissADME: a free web tool to evaluate pharmacokinetics, drug-likeness and medicinal chemistry friendliness of small molecules, Sci. Rep. 7 (2017) 42717.
[60] G.M. Morris, R. Huey, W. Lindstrom, M.F. Sanner, R.K. Belew, D.S. Goodsell, A. J. Olson, AutoDock4 and AutoDockTools4: Automated docking with selective receptor flexibility, J. Comput. Chem. 30 (2009) 2785–2791.
[61] F. Qiao, L. Luo, H. Peng, S. Luo, W. Huang, J. Cui, X. Li, L. Kong, D. Jiang, D. J. Chitwood, D. Peng, R.F. Waller, Characterization of Three Novel Fatty Acid- and Retinoid-Binding Protein Genes (Ha-far-1, Ha-far-2 and Hf-far-1) from the Cereal Cyst Nematodes Heterodera avenae and H. filipjevi, PLoS One 11 (8) (2016) e0160003.
[62] J. Gasteiger, M. Marsili, Iterative partial equalization of orbital electronegativity—a rapid access to atomic charges, Tetrahedron 36 (1980) 3219–3228.
[63] C.J. Millard, P.J. Watson, I. Celardo, Y. Gordiyenko, S.M. Cowley, C.V. Robinson, L. Fairall, J.W. Schwabe, Class I HDACs share a common mechanism of regulation by inositol phosphates, Mol. Cell 51 (2013) 57–67.
[64] J. Liu, Y. Yu, J. Kelly, D. Sha, A.B. Alhassan, W. Yu, M.M. Maletic, J.L. Duffy, D. J. Klein, M.K. Holloway, S. Carroll, B.J. Howell, R.J.O. Barnard, S. Wolkenberg, J. A. Kozlowski, Discovery of Highly Selective and Potent HDAC3 Inhibitors Based on a 2-Substituted Benzamide Zinc Binding Group, ACS Med. Chem. Lett. 11 (2020) 2476–2483.
[65] P.J. Watson, L. Fairall, G.M. Santos, J.W. Schwabe, Structure of HDAC3 bound to co-repressor and inositol tetraphosphate, Nature 481 (2012) 335–340.
[66] C.A. Luckhurst, O. Aziz, V. Beaumont, R.W. Burli, P. Breccia, M.C. Maillard, A. F. Haughan, M. Lamers, P. Leonard, K.L. Matthews, G. Raphy, A.J. Stott, I. Munoz-Sanjuan, B. Thomas, M. Wall, G. Wishart, D. Yates, C. Dominguez, Development and characterization of a CNS-penetrant benzhydryl hydroxamic acid class IIa histone deacetylase inhibitor, Bioorg. Med. Chem. Lett. 29 (2019) 83–88.
[67] Y. Hai, D.W. Christianson, Histone deacetylase 6 structure and molecular basis of catalysis and inhibition, Nat. Chem. Biol. 12 (2016) 741–747.
[68] A. Schuetz, J. Min, A. Allali-Hassani, M. Schapira, M. Shuen, P. Loppnau, R. Mazitschek, N.P. Kwiatkowski, T.A. Lewis, R.L. Maglathin, T.H. McLean, A. Bochkarev, A.N. Plotnikov, M. Vedadi, C.H. Arrowsmith, Human HDAC7 harbors a class IIa histone deacetylase-specific zinc binding motif and cryptic deacetylase activity, J. Biol. Chem. 283 (2008) 11355–11363.
[69] A.A. Tabackman, R. Frankson, E.S. Marsan, K. Perry, K.E. Cole, Structure of 'linkerless' hydroxamic acid inhibitor-HDAC8 complex confirms the formation of an isoform-specific subpocket, J. Struct. Biol. 195 (2016) 373–378.
[70] G.L. Warren, T.D. Do, B.P. Kelley, A. Nicholls, S.D. Warren, Essential considerations for using protein-ligand structures in drug discovery, Drug Discov. Today 17 (2012) 1270–1281.
[71] U.C. Singh, P.A. Kollman, An approach to computing electrostatic charges for molecules, J. Comput. Chem. 5 (2) (1984) 129–145.
[72] G. Floresta, E. Amata, C. Barbaraci, D. Gentile, R. Turnaturi, A. Marrazzo, A. Rescifina, A structure-and ligand-based virtual screening of a database of "small" marine natural products for the identification of "blue" sigma-2 receptor ligands, Mar. Drugs 16 (10) (2018) 384.
[73] D. Santos-Martins, S. Forli, M.J. Ramos, A.J. Olson, AutoDock4(Zn): an improved AutoDock force field for small-molecule docking to zinc metalloproteins, J. Chem. Inf. Model. 54 (8) (2014) 2371–2379.